Experimental Study of Flow Patterns and Pressure Drop in Cocurrent Gas-liquid Down Flow in a Packed Column

A Thesis

Presented to

the Faculty of the Department of Chemical and Biomolecular Engineering

University of Houston

In Partial Fulfillment

of the Requirements for the Degree

Bachelor of Science

in Chemical Engineering

by

Christine E Stroh

May 2019

Experimental Study of Flow Patterns and Pressure Drop in Cocurrent Gas-liquid Down Flow in a Packed Column

_____
Christine Stroh

Approved:

_____
Chair of the Committee
Dr. Vemuri Balakotaiah, Professor,
Chemical and Biomolecular Engineering

Committee Members:

_____
Dr. Jacinta C Conrad, Professor,
Chemical and Biomolecular Engineering

_____
Dr. Frank J Claydon, Professor,
Electrical and Computer Engineering

_____
Dr. Suresh K Khator, Associate Dean,
Cullen College of Engineering

_____
Dr. Michael Harold, Professor and Chair,
Chemical and Biomolecular Engineering

Acknowledgements

I would like to acknowledge Dr. Vemuri Balakotaiah for letting me use his lab and equipment for this thesis, Dr. Paul Salgi for assisting me in the lab, my parents (Dr. Friedemann Stroh and Dr. Bernice Allen-Stroh) for helping me narrow down a topic for this thesis, Gerald Blosser for assisting Dr. Salgi and me in the lab, and my thesis committee (Dr. Balakotaiah, Dr. Jacinta Conrad, and Dr. Frank Claydon) for helping me experience doing a thesis as an undergraduate.

Experimental Study of Flow Patterns and Pressure Drop in Cocurrent Gas-liquid Down Flow in a Packed Column

An Abstract

of a

Thesis

Presented to

the Faculty of the Department of Chemical and Biomolecular Engineering

University of Houston

In Partial Fulfillment

of the Requirements for the Degree

Bachelor of Science

in Chemical Engineering

by

Christine E Stroh

May 2019

Abstract

Packed bed columns are widely used throughout many chemical processes to carry out reactions between gas and liquid reactants requiring a solid catalyst. Flow patterns and their associated pressure drops are two important parameters that can optimize the operation of these reactors. However, the analysis of these parameters is usually above the understanding of the operators who control the reactors. This thesis evaluates these parameters in a laboratory scale packed column, compares the results to literature values, and analyzes the data in a simpler way using parameters easily found with equipment in a chemical plant. The experimental data reasonably fit the well-known Tosun flow map and a modified Lockhart-Martinelli correlation. New analysis showed that when plotted as a pressure trace standard deviation normalized by its average versus its gas flow rate, the data had a visual change in slope whenever the flow pattern transitioned, giving operators a simpler way to identify transitioning flows.

Table of Contents

List of Figures

List of Tables

Nomenclature Table

Table 1: Nomenclature.

Parameter Symbol	Definition
A	Cross-sectional area
Avg	Average
C	Constant
D	Diameter of the column (0.0508 m)
d_p	Diameter of the packing particle (3 mm)
(Flux)	Mass flux of either liquid or gas
G	Gas flow rate
G_{flux}	Gas mass flux
Hp	Horsepower
ID	Inner diameter
kg	Kilograms
L	Length
L_{Flux}	Liquid mass flux
L/min	Liters per minute
m	Meters
mm	Millimeters
Pa	Pascal
psia	Pounds per square inch absolute
PT1	Pressure transducer 1
PT1-4	PT1 to PT4
PT2	Pressure transducer 2
PT2-4	PT2 to PT4
PT3	Pressure transducer 3
PT4	Pressure transducer 4
Q	Flow rate
R	Gas constant
Re	Reynolds number

rpm	Revolutions per minute
s	Seconds
SS	Stainless steel
Std	Standard deviation
Subscript bead	Packing
Subscript col	Column
Subscript G	Gas
Subscript L	Liquid
Subscript LG	Liquid-gas (two-phase flow)
T	Temperature
u	Superficial velocity
V	Volume
VDC	Voltage with direct current
φ	Phi from Lockhart-Martinelli
X	Chi from Lockhart-Martinelli
ΔP	Change in pressure
ρ	Density
ε	Porosity
μ	Dynamic viscosity

1. Introduction

When observing flow patterns and transitions in laboratory packed bed columns, dimensionless parameters, mass fluxes, pressure drops, and other expressions are usually used for analysis. In the engineering industry, plant operators usually only have flow rates and pressure drops available to them because these parameters are easily accessible from infield equipment. If flow pattern is essential to a process in a packed column but the plant operator cannot look into the column to see the flow pattern, operators would need to do extensive analysis or have an extensive analysis program setup to analyze the flow pattern. However, they might not understand how the program works. (Most plant operators do not have an engineering background.) The purpose of this thesis is to find a way to determine when flow patterns are transitioning from pulse to bubbly flow or pulse to trickle flow based on parameters that are easily measured and found in an engineering plant: average pressure, standard deviation of pressure, and gas flow rate. If plant operators have a method to identify when flow patterns are changing that they understand, they can more confidently and knowledgably fix the problem and optimize the packed column. Also, process engineers could have another method of analysis for determining flow pattern transitions.

This thesis observes pressure traces and pressure drops throughout a cocurrent downward flow, air-water packed column. The flow regimes ranged from trickle to pulse to bubbly. Pressure drop and analytical analysis were done to compare these experiments to past, published experiments and correlations for accuracy purposes. Then, visual standard deviation normalized by an average versus gas flow rate analysis was completed to see if these parameters could be used to show a transition in flow pattern.

Background

Packed beds are widely used throughout the chemical, petrochemical, and biochemical industries. A packed bed's defining feature is its packing, which separates it from trayed or open pieces of equipment. The packing can be a variety of shapes and sizes from spheres to rings and coils. A common application of the packing in these columns is catalyst support. Because the catalyst is usually in the solid phase and both gas and liquid can flow cocurrently or countercurrently through the column, the packed bed would be a three-phase reactor. To operate and optimize this reactor, the design engineer usually needs information about flow patterns,

liquid holdup, and pressure drop. Because this information is not always available, due to the absence of a theoretical model, the design engineer relies on experimental correlations to determine these hydrodynamic quantities [1]. Correlations are usually developed and calculated using lab scale columns, but their accuracy diminishes outside of specific conditions. Therefore, basic experiments with air, water, and a uniform packing are a good starting point for understanding how packed beds work, and adjustment to models are made as they are introduced into the process.

This thesis specifically observes pressure drops in a nonreactive, cocurrent, two-phase downward flow packed column, meaning that the liquid and gas enter the column on the same side and both exit the column on the other side. With both liquid and gas flowing through the packed column, the interactions between the liquid and gas (flow pattern) are difficult to calculate analytically, so they are observed experimentally as visual patterns or via pressure traces. Packed columns with cocurrent downward flow usually have the following flow patterns: bubbly, spray, trickle, and pulse [2]. Due to constraints with rotameters, only bubbly, trickle, and pulse flows were observed with this packed column. Figure 1 and Figure 2 show visually how each of the three flow patterns looks. In Figure 1, the trickle flow coats the packing in liquid while the gas makes up the continuous phase. Bubbly flow has air bubbles surrounded by a continuous liquid phase. Pulse flow has alternating gas and liquid phases that move or pulse down the column. In Figure 2, the left side of the figure shows pulse flow throughout the column. Regions of mixed gas and liquid (shown in green) build up pressure, alleviate the pressure by moving through a section of the column, build up pressure, alleviate pressure by moving through a section of the column, etc., causing a “pulse” throughout the column. The center of Figure 2 shows bubbly flow throughout the entire column. The right side of Figure 2 shows trickle flow throughout the entire column. At low enough flow rates, trickle flow can sometimes look like nothing is flowing through the column.

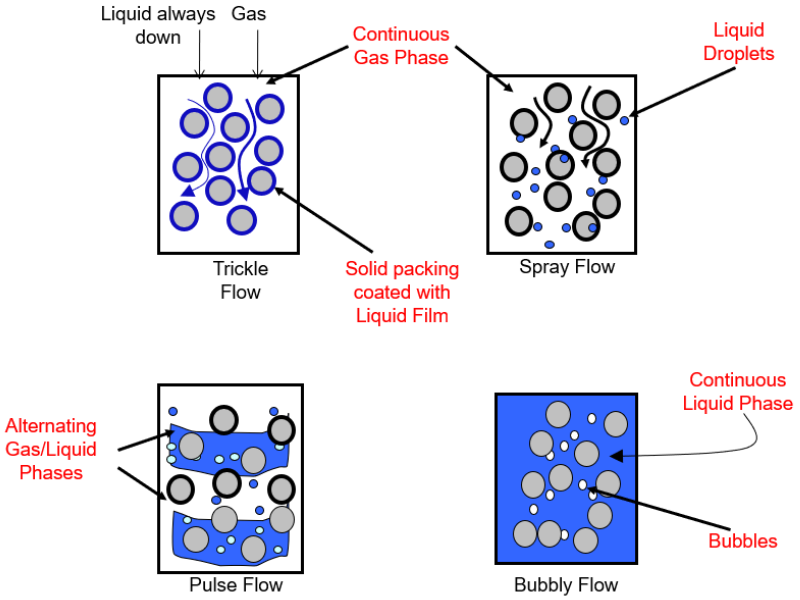

Figure 1: Schematic representation of flow patterns in a downward cocurrent packed column [3].

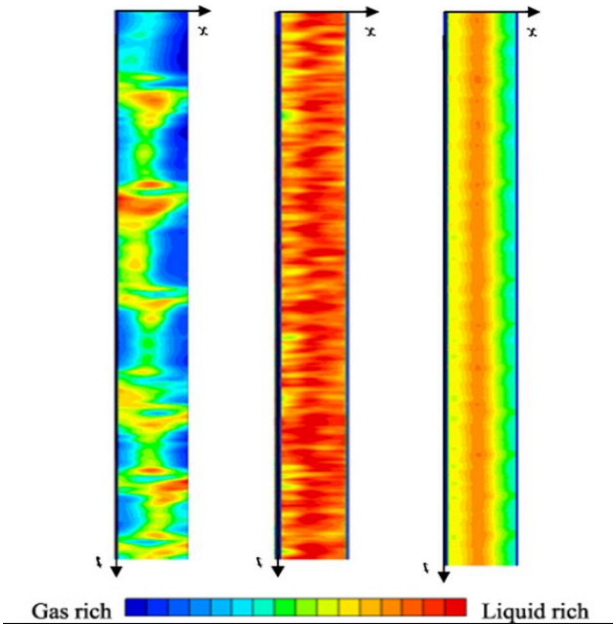

Figure 2: Visual representation of flow patterns. The left column demonstrates pulse flow. The center column demonstrates bubbly flow. The right column demonstrates trickle flow. The t axis represents the center of the column, so only half of the column diameter is shown. The bottom of the figure explains the color gradient inside each column [4].

Flow patterns can also be recognized through pressure traces. A pressure trace is a graph that records the pressure at a fixed location over a period of time. Pressure traces are usually more accurate in identifiying flow patterns than visual recognition because analytical oscillations can be compared instead of relying on the human eye to identify differences and transition points. Figure 3 shows the pressure trace of pulse flow. Because pulse flow continually builds up pressure and then decreases the pressure, the pressure trace has relatively large oscillations compared to bubbly or trickle flow. Figure 3 specifically has more than a 1 psia pressure change with its oscillations. Figure 4 shows the pressure trace for bubbly flow. Compared to pulse flow, bubbly flow's oscillations are signinifcantly smaller and in Figure 4 are less than 0.1 psia. In addition, the average pressure is lower for bubbly flow compared to pulse flow. Figure 5 shows the pressire trace for trickle flow. Trickle flow has approximately no oscillations (less than 0.05 psia in Figure 5) and the average pressure is lower than both bubbly and pulse flow.

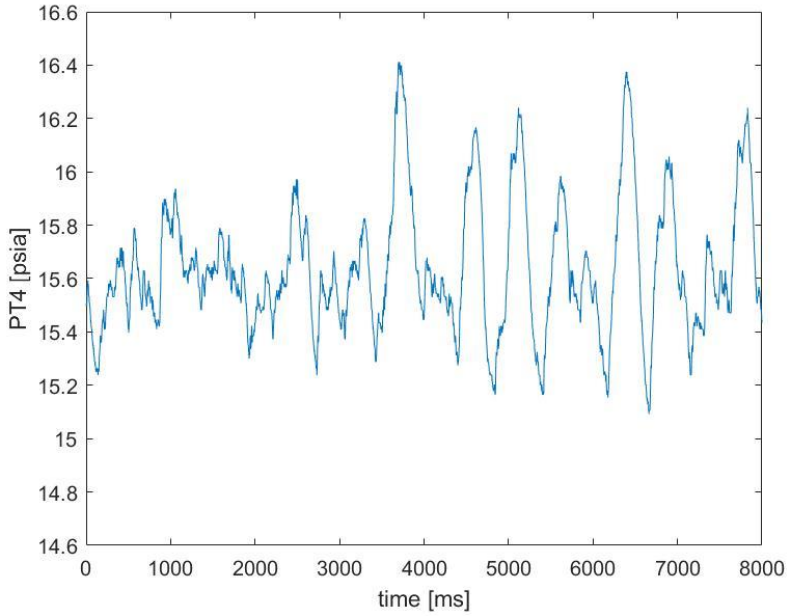

Figure 3: Typical pressure trace from pulse regime. Pulse flow has defined oscillations as the pressure builds up and decreases with each pulse. The pressure range is larger than that of bubbly or trickle flow. The y-axis is larger than the data to compare the pulse pressure trace to the trickle pressure trace and bubbly pressure trace at the same range.

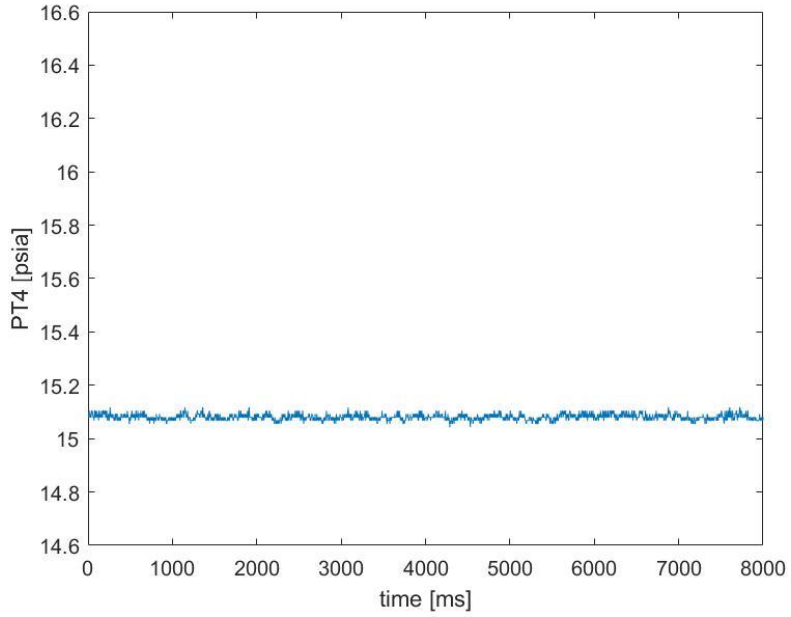

Figure 4: Typical pressure trace from bubbly regime. The y-axis is larger than the data to compare the bubbly pressure trace to the trickle pressure trace and pulse pressure trace at the same range. The bubbly flow pattern does not have defined oscillations like in pulse flow, but it has more pressure movement than trickle flow.

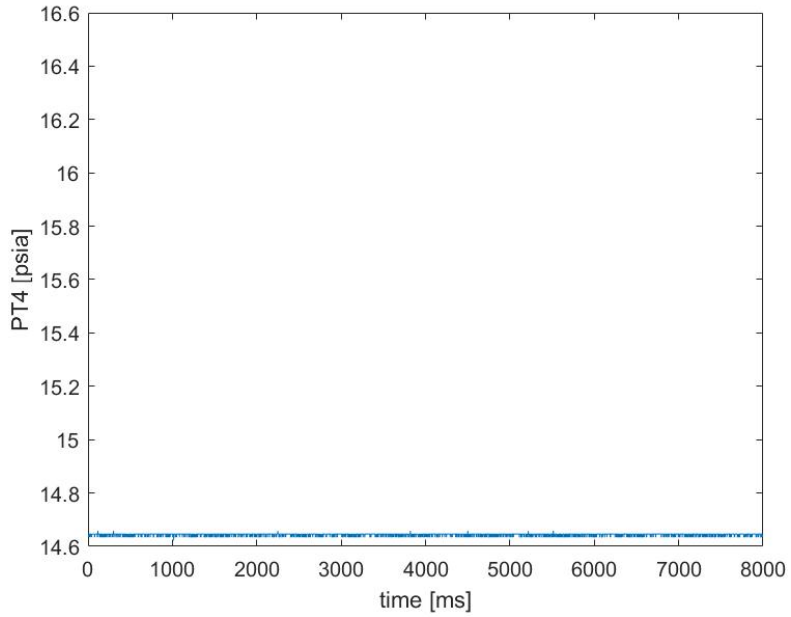

Figure 5: Typical pressure trace for trickle regime. The y-axis is larger than the data to compare the trickle flow to the bubbly and pulse flow at the same range. Trickle flow has almost no change in pressure compared to bubbly and pulse flow. In addition, the relative pressure is lower than pulse or bubbly flow.

Flow in a packed bed can transition from pulse to bubbly flow or pulse to trickle flow. The transitions express qualities of both flow patterns. In Figure 6, the transition between pulse and trickle has a higher average pressure than trickle flow, but smaller oscillations compared to pulse flow.

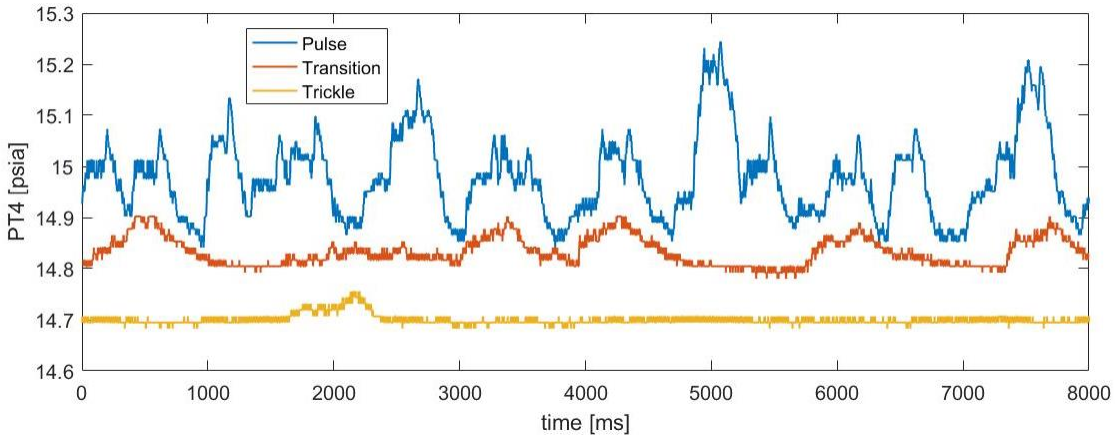

Figure 6: Pressure trace transition from pulse to trickle flow. The transition has features from both pulse and trickle flow.

In Figure 7, the transition from pulse to bubbly oscillates more than the transition from pulse to trickle and has a higher average pressure than bubbly flow. The bubbly flow in Figure 7 may be confused with trickle flow because the oscillations cannot be seen on the same scale as pulse flow, but one way to differentiate Figure 6 and Figure 7 is the relative pressure and oscillation size.

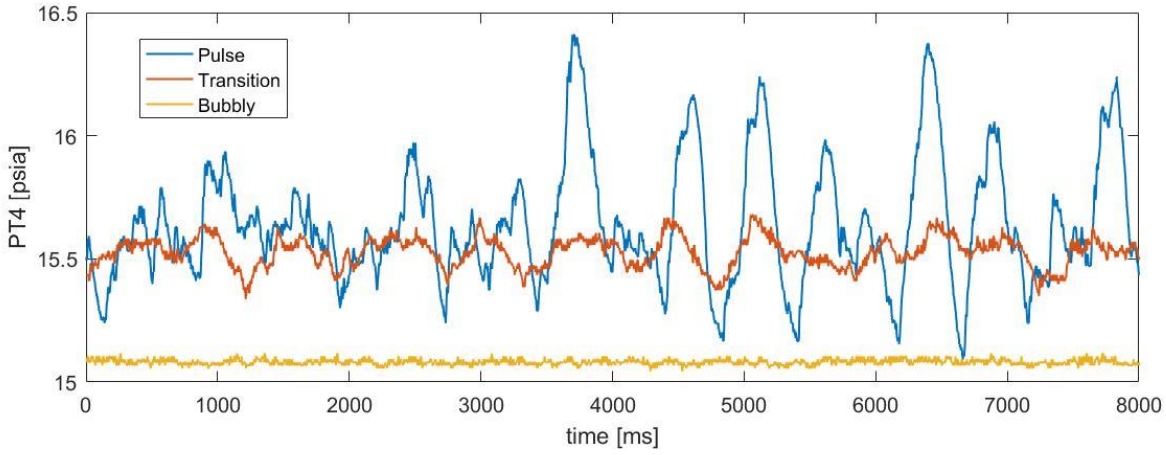

Figure 7: Pressure trace transition from pulse to bubbly flow. The transition has a higher average pressure than the bubbly flow and more defined oscillations, but the oscillations are smaller than the pulse oscillations.

Compared to analytically defined transitions, visually, the column will have characteristics of both flows when it is transitioning. Overall, it is more difficult to visually identify transitions with the human eye than to analyze the traces using statistical techniques.

Each type of flow pattern depends on the gas and liquid flow rates. Because the packing and porosity also affect the transition points between types of flow [2], flow maps, as shown in Figure 8, should be determined experimentally. The most practical way to map the flow regimes is with a test matrix. For example, a test matrix can hold the liquid flow rate constant while increasing the gas flow rate at certain increments so that the flow patterns can be recorded. This procedure is repeated at different liquid flow rates.

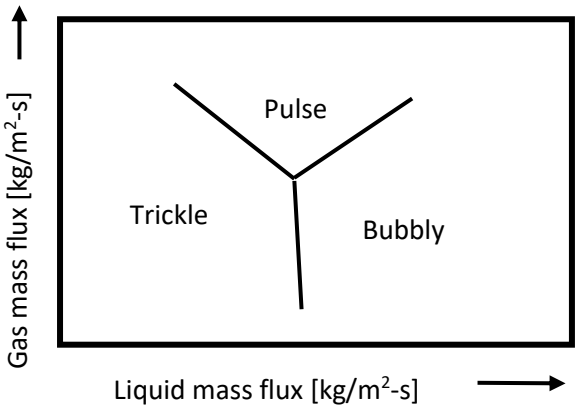

Figure 8: A generic flow map. The pulse, bubbly, trickle, and transition flow patterns are determined experimentally and graphed using the gas and liquid mass fluxes.

Once water is run through the column, the column remains wet; therefore, a gas only pressure drop reading would not be accurate. Pressure drop of a single-phase experiment in a packed column can be predicted with empirical correlations; however, the accuracy of such correlations changes as the conditions within the column change. If a column is packed with spheres, the Ergun correlation, Equation(3), can be used to predict the gas only pressure drop [5]. Usually the constants used in the Ergun equation are 150 and 1.75, but reference [3] determined 118.2 and 1.0 provided better data when using the Ergun equation with the Lockhart-Martinelli correlation, so those coefficients were used.

The Lockhart-Martinelli correlation predicts and compares pressure drops in inertially dominated flows. Reference [6] explains how pressure drop can be used instead of constants,

correlations, and dimensionless parameters, which makes for an easier analysis. Because either the gas or liquid can dominate the flow and the flow can be viscous or turbulent, Figure 9 compares the differences graphically. Viscous flow is estimated to occur for Re less than 1000 while inertially dominated flow is estimated to occur for Re greater 2000 [6]. Figure 10 compares the accuracy of different gas and liquid components with the correlation, showing that a majority of the points are within 14% of the calculated value. Finally, Figure 11 compares the correlation to other correlations, showing that Lockhart-Martinelli is a reasonable correlation to use to graph inertially based pressure drops.

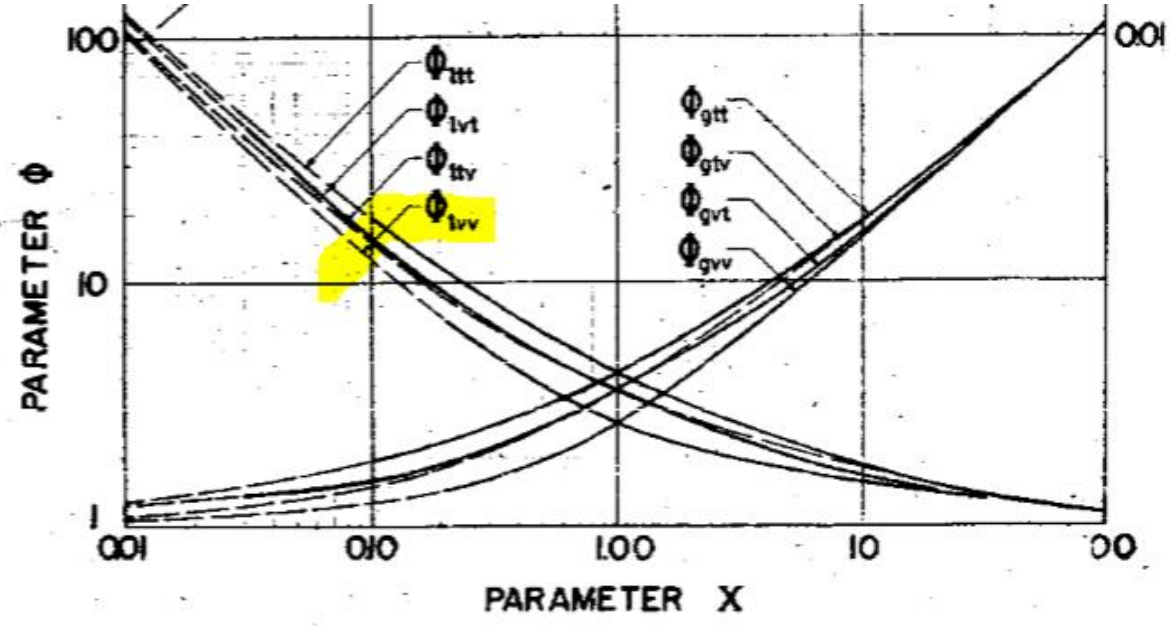

Figure 9: Lockhart-Martinelli comparing viscous (v) and turbulent (t) flows in liquid dominated (l) and gas dominated (g) regimes [6]. The liquid dominated viscous-viscous curve is mostly used in this thesis.

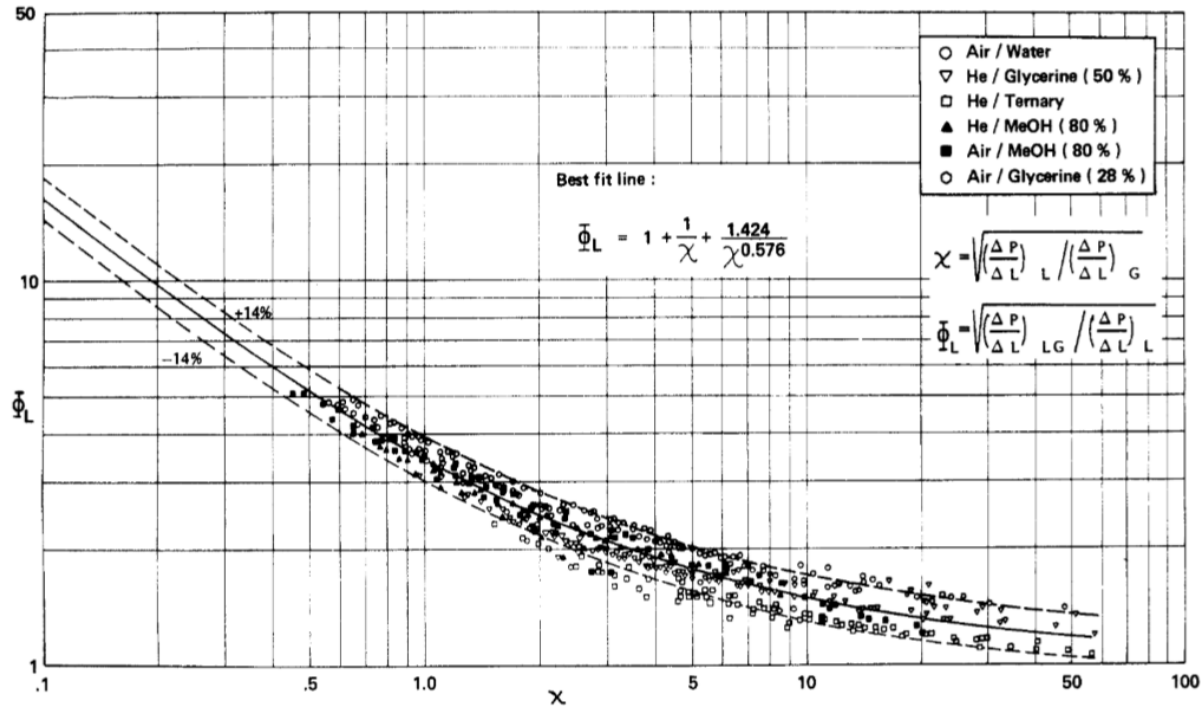

Figure 10: Lockhart-Martinelli as determined by reference [7].

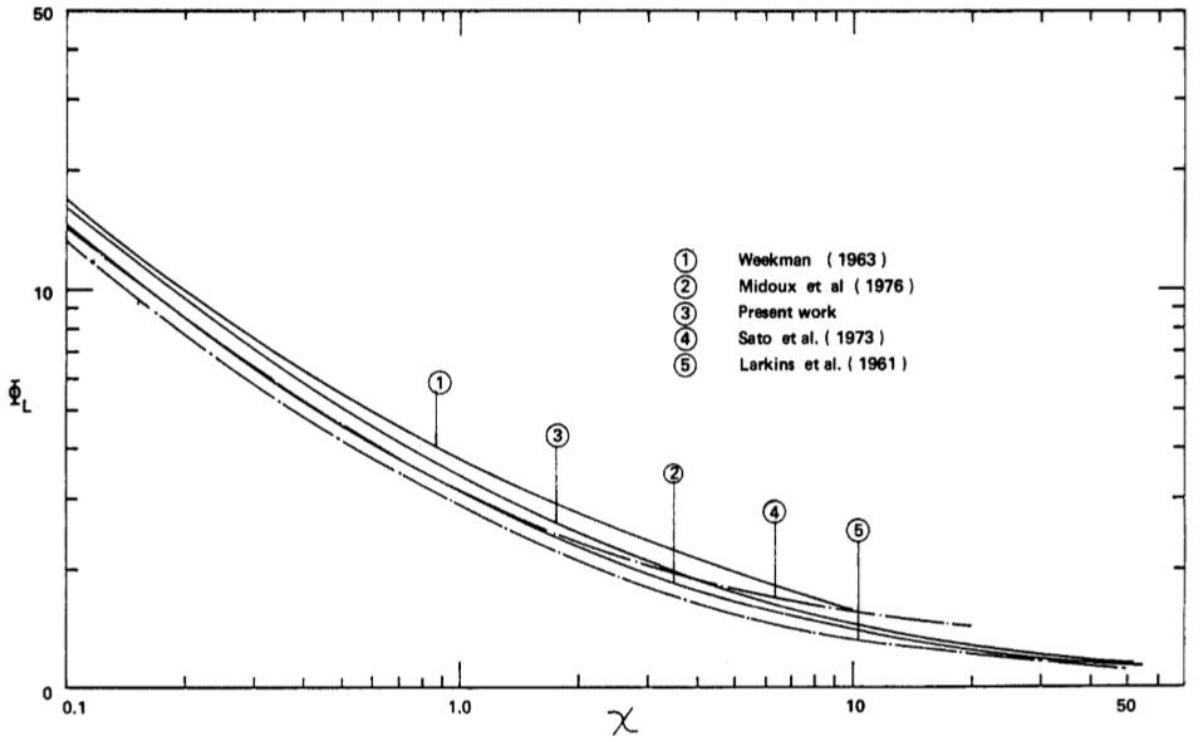

Figure 11: Lockhart-Martinelli compared to other correlations [7]. "Present work" was the Lockhart-Martinelli correlation as determined by [7].

Before the liquid and gas can even cause a pressure drop throughout the column, they first have to enter the column and pass a distribution plate. Distribution plates are usually placed at the entrance of packed columns to uniformly mix the gas and liquid before they reach the packing [8]. If the liquid and gas do not mix well before entering the column, hot spots (for reactions) and/or less defined, maldistributed flow patterns can form, decreasing the efficiency of the column and possibly decreasing the safety of the column. Also, the mass transfer and correlation predictions will be less accurate because the nonideality of nonuniform mixing cannot be taken into account with simulations [1]. Therefore, the packing of the column should touch the distribution plate to minimize entrance effects.

2. Experimental Setup

First Experiment of the Day

Before experiments could be run, the electronics and column needed to be setup. To start, the water container was filled with approximately 5 gallons of water. The water line drained into a drain for a few minutes before collecting water in the container in case rust settled in the tap water line. The pump tubing was connected to the container. The lid was put onto the container such that the bottom of the column emptied into the water container. The pump driver and two 12-volt boxes were plugged into an outlet. The volt boxes were turned on and adjust to 12 VDC. The laptop was turned on, and the two USBs from the data boxes were connected to the laptop. The software on the laptop was opened. The valve positions on the tubing were adjusted to the high flow rotameters, for both liquid and gas. Now, the setup was ready for the column warmup.

Column Warmup

Before the first experiment of the day or between experiments of different liquid flow rates, the column warmup was followed to ensure each set of experiments started with the same column conditions. The pump was turned on, and the driver and liquid rotameter were adjusted until a liquid flow rate of at least 2.5 L/min was reached. The liquid ran through the column for at least 5 minutes. During those 5 minutes, the gas rotameter was checked to ensure it was closed, and the values were checked to ensure they were in the correct position (only allowing flow to the high rotameter). After the 5 minutes, the air regulator was used to start the air flow. Slowly, the air flow rate on the air rotameter increased until the column was pulsing. The column pulsed for 1 minute. (If desired, the TracerDAQ software could be run to make sure it worked properly.) After the 1 minute, the gas flow was reduced to the minimum on the gas rotameter. The liquid flow rate was set to the desired flow rate, changing the valves/rotameters if necessary. The gas flow rate was set to 17 L/min. Now the desired experiments could be run.

Experimental Procedure

Once the desired liquid and gas flow rates were reached, at least 2 minutes were given for the flow rates and column to stabilize. Toward the end and after this 2-minute period, the gauge pressure (or range of pressures), using the pressure gauge located on the air line, was

observed and recorded. Once the gauge pressure (ranges) was (were) recorded and it has been at least 2 minutes, the TracerDAQ software ran. The raw data was saved as a CSV file. Depending on the next experiment, either the gas flow rate was adjusted and the experimental procedure was repeated, or the column warmup was repeated for the next set of experiments. Experiment sets were run at liquid flow rates of 3 L/min, 2 L/min, 1.5 L/min, 1.2 L/min, and 1 L/min. At each liquid flow rate, 8 different gas flow rates were tested in decreasing magnitude: 17 L/min, 15 L/min, 11 L/min, 7 L/min, 5.5 L/min, 3.5 L/min, 2.5 L/min, and 0 L/min. Because both the high and middle rotameters were used for gas flow rates, 7 L/min was run twice, once on the high rotameter and once on the middle rotameter.

If an atmospheric reading needed to be done for pressure transducer calibration adjustments, the pump was turned off to stop the water flow. Then, air was used to push as much water out of the column as possible. The air was turned off so that nothing was flowing through the column, and then the software took readings.

Shutdown Procedure

After the last experiment was run, the air was shut off using the air regulator. The liquid flow was stopped by turning off the pump. As the liquid drained from the column, the files were checked, making sure they were saved to the external hard drive. The software was exited, the volt boxes were shut off, and their cords were unplugged. The pump driver electrical cord and data box USB cords were also unplugged. The water was emptied from the container into the drain, and the container dried upside down. The volt boxes were covered with a plastic sheet, and the general setup was checked so that the area looked organized.

Air Leak Procedure

Because the valves and connections on the air side of the process could leak, a liquid leak detector called Snoop was applied to each rotameter connection (top and bottom) and valve connection. If the connection was not airtight, the leak detector formed bubbles. During an experiment, if bubbles formed, the experiment was stopped, and the system was shutdown. The leaking connection was taken apart, and the Teflon tape was rewrapped. The connection was put back together, and air was run through the system to make sure the leak was stopped. Once the leak detector did not form anymore bubbles, the experiment restarted. If bubbles still formed,

the Teflon tape was rewrapped again, and the tubing was adjusted to see if a better angle of connection could fix the problem.

Equipment Specifics

This section will describe the specifics of the equipment used for the experiments. Figure 12 shows the specifics for the column. The column had a 2-inch ID and 0.25-inch wall thickness. The inlet thread of the column was 0.5 inch while the outlet thread of the column was 1 inch. The packing inside the column was 3 mm (+/- 10%) soda lime glass beads by Sigma Aldrich and spanned approximately 5 feet and 1 inch. PT1 was located approximately 2 inches below the top of the packing, PT2 was located approximately 11 inches below PT1, PT3 was approximately 21 inches below PT2, and PT4 was located approximately 21 inches below PT3 (or 6 inches above the bottom of the packing). The column had one distributor plate resting above the packing and a meshing at the bottom of the packing. The distributor plate was 0.036 inches thick 304 SS with 0.125-inch holes staggered 0.1875 inches apart. The holes made up 40% of the plate. The bottom mesh was 70% open space T 316 SS 18 mesh with a wire diameter of 0.009 inches.

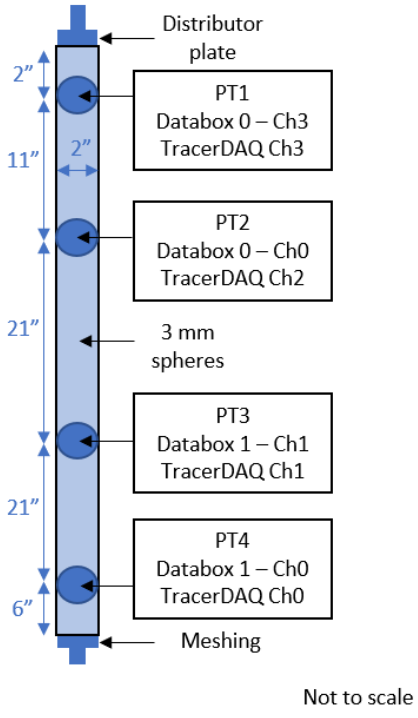

Figure 12: Column information. Note that the drawing is not to scale.

PT1, PT2, and PT3 were from Cole-Palmer and ranged from 0-50 psia (0.2-5.2 VDC). PT4 was also from Cole-Palmer but ranged from 0-25 psia (0.2-5.2 VDC). The pressure transducers came pre-calibrated from the company with a linear correlation to convert the voltage reading to pressure. The volt boxes that powered the pressure transducers were from BK Precision. They supplied a 12 VDC with 0.5 amps. The databoxes that transferred the voltage reading to the laptop were from Cole-Palmer, and the software used to observe and save the data was TracerDAQ.

Teflon tubing (~0.5-inch) was used to transfer water and air into the column with Apollo International lead free, quarter-turn valves. (The valves appeared to be ball valves, but because the valves were either open or closed, the type of valve was not important to identify.) Even though three gas and three liquid rotameters were connected to the column, only four of the six rotameters were used for experiments: the "high" liquid, the "medium" liquid, the "high" gas, and the "medium" gas. The high liquid rotameter was from Dakota and marked from 1 L/min to 4 L/min with 5%-10% error. The medium liquid rotameter was from Omega and marked from 0.1 L/min to 2.0 L/min with 5%-12% error. The pump used to circulate the water was an Inverter drive motor with 0.5 hp and 1725 rpm. A Baldor adjustable speed drive was used to control the speed. For the gas side of the process, Matheson Tri-gas, nonflammable compressed air and regulator were used. The high gas rotameter was from Omega and marked from 1 L/min to 17 L/min with 5%-11% error. The medium gas rotameter was from Dakota and marked from 7.467 L/min to 0.389 L/min with 2%-9% error. The gas pressure gauge on the air line was from SSI Technologies Inc.

Materials

The materials used in the experiments were water, compressed air, packing (spheres), column (with distribution plate and end caps), 4 pressure transducers, 2 data boxes, 2 volt boxes, Excel, TracerDAQ, inscal32 (to install the databoxes), Matlab, 2 liquid rotameters, 2 gas rotameters with correction factors, Teflon tubing, check valves, valves, large container with a lid to hold/collect water, stand to hold column and electronics, laptop, external hard drive, pump and driver, a pressure gauge, personal protective equipment (safety glasses, lab coat, closed-toed shoes), liquid leak detector, general toolkit with wrenches and screw drivers, and Teflon tape.

Setup

As shown in Figure 13 and Figure 14, water and air entered the column from the top. The water and air exited the column from the bottom where the air was released to the atmosphere and the water was collected in a container. The collected water was then pumped through the tubing to a three-way split. Depending on which rotameter was in use, the water flowed through one of the three valves. After the rotameter, the water traveled through the secondary valve where the three valves reconnected. The water then traveled through a check valve and then entered the column. Air from an air canister traveled through a similar process. The air moved to the three-way split and continued through whichever valve was open, through a rotameter, and then reconnected with the remaining two pathways. The air then traveled through a pressure gauge and then through a check valve, where it then entered the column. Note that only two out of the three liquid rotameters were used and only two out of the three gas rotameters were used.

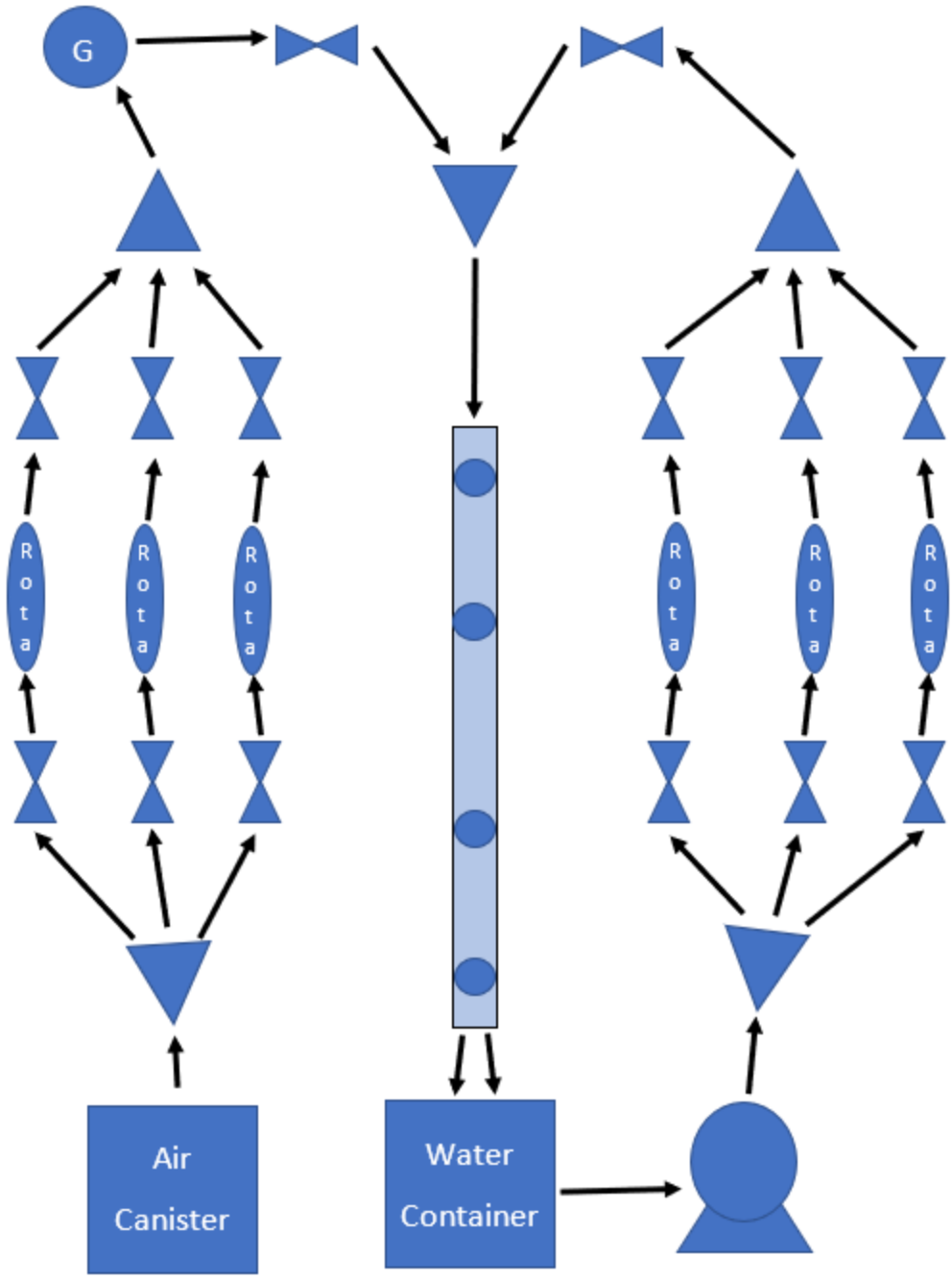

Figure 13: Schematic of flow setup. "Rota" stands for rotameter. "G" stands for pressure gauge. The rectangle with 4 circles above the water container is the column and pressure transducers, respectively. The triangles represent when the tubing splits or rejoins. The driver of the pump is connected to a power source, an outlet, which is not shown in the diagram. Even though a total of six rotameters were connected to the column, only two gas and two liquid rotameters were used for experiments.

Figure 14: Photograph of experimental setup.

As shown in Figure 15, each of the four pressure transducers sent signals to two data boxes. The data boxes were powered by voltage boxes and sent the pressure transducer signal to the laptop via two USBs.

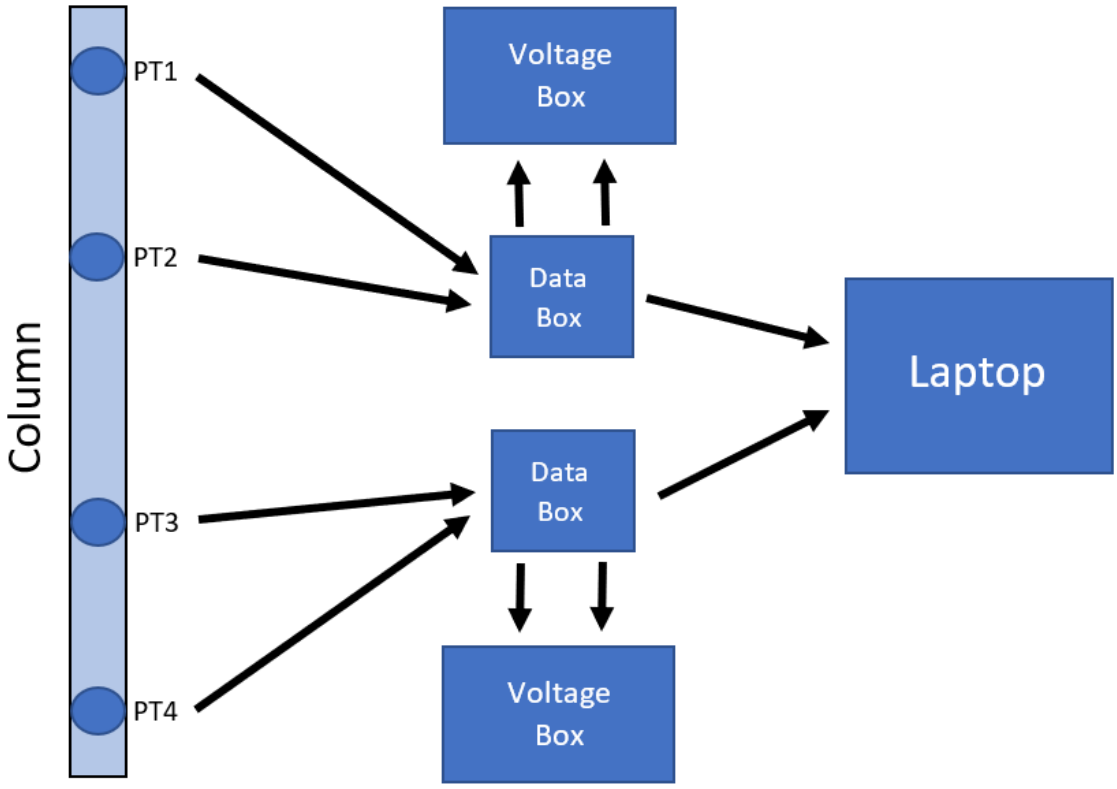

Figure 15: Diagram of data collection. Each data box is connected to two pressure transducers and one voltage box. The voltage boxes are plugged into an outlet for power. Each data box is connected to the laptop via USB.

3. Results and Discussion

The experiments were analyzed in different ways for accuracy and comparison to literature values. Then, the experiments were plotted by the PT4 pressure trace standard deviation normalized by its average versus its gas flow rate to see if this simpler method could visually identify changes in flow patterns. (PT4 was chosen because it should trace the most developed flow.) Before the experiments could be analyzed, their data needed to be converted into a usable form and specific correlation parameters needed to be calculated, as shown in the Raw Data Analysis and Extrapolation sections. The data were then analyzed and compared in the PT3, Packing, Flow Matrix, Lockhart-Martinelli Correlation, and Pressure Gradient Analysis sections. Because the experiments were going to be analyzed in an unfamiliar way in the Standard Deviation/Average Versus Gas Flow Rate section, it was important to make sure that the data reasonable compared to known methods of evaluation and the analysis logically made sense. Finally, in the Standard Deviation/Average Versus Gas Flow Rate section, the data were analyzed using PT4's standard deviation normalized by its average versus its gas flow rate to see if this relatively simple method of analysis could show or predict flow pattern transitions.

Raw Data Analysis

Because the pressure transducers measure pressure changes with a voltage signal, the raw data needed to be converted to a pressure value using a linear correlation provided by the manufacturer. See Figure 64, Figure 65, Figure 66, and Figure 67 in the Appendix E under Cole-Palmer Calibration Curves. An example of how the raw data looked is shown in Table 2. Each pressure transducer recorded a total of 28,000 points for a total of 28 seconds.

Table 2: Example of raw data from each of the four pressure transducers using TracerDAQ software. The voltage values are in columns C-F. These columns have four decimal places to track the minute changes in pressure for better accuracy and precision for when these values are converted to pressures.

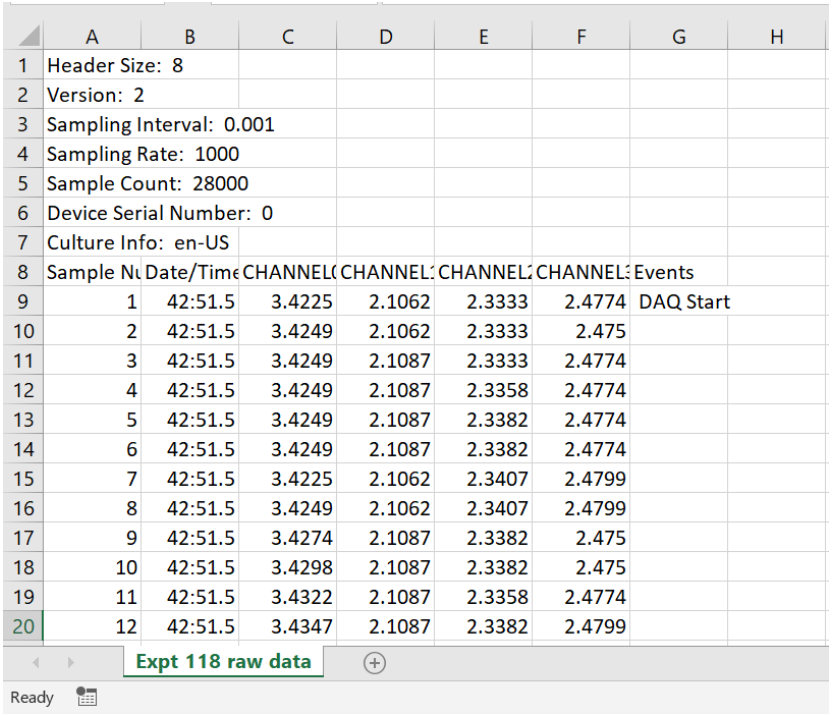

	A	B	C	D	E	F	G	H
1	Header Size: 8							
2	Version: 2							
3	Sampling Interval: 0.001							
4	Sampling Rate: 1000							
5	Sample Count: 28000							
6	Device Serial Number: 0							
7	Culture Info: en-US							
8	Sample Nu	Date/Time	CHANNEL(	CHANNEL:	CHANNEL:	CHANNEL:	Events	
9	1	42:51.5	3.4225	2.1062	2.3333	2.4774	DAQ Start	
10	2	42:51.5	3.4249	2.1062	2.3333	2.475		
11	3	42:51.5	3.4249	2.1087	2.3333	2.4774		
12	4	42:51.5	3.4249	2.1087	2.3358	2.4774		
13	5	42:51.5	3.4249	2.1087	2.3382	2.4774		
14	6	42:51.5	3.4249	2.1087	2.3382	2.4774		
15	7	42:51.5	3.4225	2.1062	2.3407	2.4799		
16	8	42:51.5	3.4249	2.1062	2.3407	2.4799		
17	9	42:51.5	3.4274	2.1087	2.3382	2.475		
18	10	42:51.5	3.4298	2.1087	2.3382	2.475		
19	11	42:51.5	3.4322	2.1087	2.3358	2.4774		
20	12	42:51.5	3.4347	2.1087	2.3382	2.4799		

Expt 118 raw data

Ready

Using each individual calibration curve, the raw data was converted to a pressure in psia, as shown in Table 3. At atmospheric conditions (no liquid or gas flowing through the column and after air was run to remove as much water as possible), the pressure transducers' values ranged by approximately 3 psia. To adjust for this offset, each pressure transducer was compared to the pressure transducer closest to 14.7 psia. Usually, this was PT1, as shown in Table 4. Because VDC is converted to psia linearly, the difference between PT1 and the other pressure transducers, during an atmospheric run, was calculated and used as their values. A new atmospheric run was taken on each day experiments were run, and air was always run through the column beforehand to ensure the column conditions were as close to atmospheric as possible. In Table 3, if the first column is column A and the second is column B and so on, columns B, E, H, and K are the raw data values; columns C, F, I, and L are the original psia values; columns D, G, J, and M are the adjusted psia values. The average of each offset pressure was calculated, and the pressure drop between different pressure transducers was calculated. Because the SI unit for pressure is Pa, the pressure drops were converted to Pa. Note that the average, standard deviation, and standard deviation divided by the average of PT4 was also calculated.

Table 3: Converting voltage to pressure. An offset was used relative to PT1, and a linear correlation on Sheet1 defined the relationship.

						avg PT1	22.81	psia	PT1 to PT2	1.22	psia			
Offset						avg PT2	21.59	psia	PT2 to PT3	4.03	psia	2.78E+04	Pa	
PT1	0.00	psia				avg PT3	17.57	psia	PT3 to PT4	1.99	psia	1.37E+04	Pa	
PT3	1.68	psia				avg PT4	15.58	psia	PT1 to PT4	7.24	psia	4.99E+04	Pa	
PT4	0.63	psia							PT2 to PT4	6.02	psia	4.15E+04	Pa	
PT2	-0.13	psia												
										Avg	Std	Std/avg		
										15.57842	0.266357	0.017098		
	Ch 3			CH 2			Ch 1			Ch 0				
	PT1			PT2			PT3			PT4				
	VDC	psia	PT1-offset	VDC	psia	PT2-offset	VDC	psia	PT3-Offset	VDC	psia	PT4-Offset		
	2.4774	22.75545	22.75545	2.3333	21.31417	21.44329	2.1062	19.07872	17.39856	3.4225	16.12393	15.49546		
	2.475	22.73145	22.73145	2.3333	21.31417	21.44329	2.1062	19.07872	17.39856	3.4249	16.13593	15.50747		
	2.4774	22.75545	22.75545	2.3333	21.31417	21.44329	2.1087	19.10373	17.42357	3.4249	16.13593	15.50747		
	2.4774	22.75545	22.75545	2.3358	21.33917	21.46829	2.1087	19.10373	17.42357	3.4249	16.13593	15.50747		
	2.4774	22.75545	22.75545	2.3382	21.36318	21.4923	2.1087	19.10373	17.42357	3.4249	16.13593	15.50747		
	Sheet1	Test Series												

Table 4: A section of Sheet1 referenced in Table 3.

PT	1	1	2	2	3	3	4	4
	VDC	psia	VDC	psia	VDC	psia	VDC	psia
	0	-2.0235	0	-2.0235	0	-1.9896	0	-0.9961
15-Nov ne	1.677853	14.75839	1.664944	14.62927	1.842262	16.43855	3.27515	15.38686
		-2.0235		-2.0235		-1.9896		-0.9961
25-Oct-18	1.6032	14.01171	1.591	13.88968	1.7961	15.97679	3.2906	15.46414

Now that the voltages from the pressure transducers were converted to Pa, other parameters could be calculated in Excel. (Matlab was used to graph the pressure traces.) Table 5 is an example of an Excel sheet used to calculate the Lockhart-Martinelli parameters. Because the Lockhart-Martinelli correlation requires a pressure drop of gas only, and the column retains too much water for a valid gas-only read, the Ergun equation was used to predict the gas-only pressure drop. The Ergun equation was chosen because it is specifically for packed beds with spherical beads and should produce reasonably accurate results. Before the Ergun equation can be calculated, the gas flow rate needed to be determined. Because the gas rotameter needs a correction factor based on the gauge pressure, the corrected gas flow rate was calculated using Equations (13) and (14). The final value was put in column G. The Ergun equation is shown in Equations (3), (6), (7), (8), (9), and (10). Table 6 shows an example of these values. Reference [9] shows that a C1 and C2 value of 118.2 and 1.0 respectively produced more accurate results, so

those C1 and C2 values were chosen. The final values were calculated in column H in Table 5. The liquid only pressure drop was experimentally determined by running liquid through the packed column and recorded in Table 5 on column I. The pressure drops calculated, as seen in Table 3, were hyperlinked to column P. Then, using Equations (1), (4), and (5), the Lockhart-Martinelli parameters were calculated in columns J, K, and O. A +/- 20% value was also calculated in columns L and M to help analyze data graphically.

Table 5: An example of determining the Lockhart Martinelli parameters for PT1-4.

A	B	C	D	E	F	G	H	I	J	K	L	M	N	O	P	Q	R
	psig	psi	Pa	L/min	L/min	L/min	Ergun 118.2	&1	Chai						Pa	m	Pa/m
Expt #		Pg + atm	Pg + atm	Q_L	Q_G	Q_G Corre	(dP/dL)G	(dP/dL)L	X	Phi_L calc	-20%	20%	PT1-4 (dP/	Phi_L expt	deltaP	deltaL	dP/dL
118	10.00	24.70	1.70E+05	3.00	17.00	22.04	736.49	8.16E+03	3.33	2.01	1.61	2.42	3.71E+04	2.13	4.99E+04	1.35	3.71E+04
119	9.70	24.40	1.68E+05	3.00	15.00	19.33	607.92	8.16E+03	3.66	1.95	1.56	2.34	3.55E+04	2.09	4.78E+04	1.35	3.55E+04
120	8.40	23.10	1.59E+05	3.00	11.00	13.79	376.80	8.16E+03	4.65	1.80	1.44	2.16	3.04E+04	1.93	4.09E+04	1.35	3.04E+04
121	6.80	21.50	1.48E+05	3.00	7.00	8.47	200.13	8.16E+03	6.39	1.65	1.32	1.98	2.43E+04	1.72	3.27E+04	1.35	2.43E+04
122	6.78	21.48	1.48E+05	3.00	7.00	8.46	199.98	8.16E+03	6.39	1.65	1.32	1.98	2.43E+04	1.73	3.28E+04	1.35	2.43E+04
123	6.16	20.86	1.44E+05	3.00	5.50	6.55	146.86	8.16E+03	7.45	1.58	1.27	1.90	2.19E+04	1.64	2.94E+04	1.35	2.19E+04
124	5.06	19.76	1.36E+05	3.00	3.50	4.06	84.77	8.16E+03	9.81	1.48	1.19	1.78	1.77E+04	1.47	2.38E+04	1.35	1.77E+04
125	4.57	19.27	1.33E+05	3.00	2.50	2.86	57.86	8.16E+03	11.88	1.43	1.14	1.71	1.57E+04	1.39	2.12E+04	1.35	1.57E+04
126	0.00	14.70	1.01E+05	3.00	0.00	0.00									1.10E+04	1.35	8.16E+03

Table 6: An example of determining the Ergun parameters. Each row corresponds to the same experiments shown in Table 5.

S	T	U	V	W	X
For Ergun	m	kg/m3	Pa-s	m/s	
	Dp	gas densit	dynamic v	superficial	porosity
	3.00E-03	2.01	1.82E-05	1.81E-01	3.53E-01
	3.00E-03	1.99	1.82E-05	1.59E-01	3.53E-01
	3.00E-03	1.88	1.82E-05	1.13E-01	3.53E-01
	3.00E-03	1.75	1.82E-05	6.96E-02	3.53E-01
	3.00E-03	1.75	1.82E-05	6.96E-02	3.53E-01
	3.00E-03	1.70	1.82E-05	5.39E-02	3.53E-01
	3.00E-03	1.61	1.82E-05	3.34E-02	3.53E-01
	3.00E-03	1.57	1.82E-05	2.35E-02	3.53E-01
	3.00E-03	1.20	1.82E-05	0.00E+00	3.53E-01

The final calculations done in Excel were to calculate both the liquid and gas fluxes and Reynolds numbers. The gas flux was calculated using Equation (12), and the liquid flux was calculated using Equation (11), as shown in column Z and column AA, respectively, in Table 7. The parameters for the gas mass flux were already calculated, but some of the parameters for the liquid mass flux needed to be determined. Because a liquid temperature of 22 C was assumed and the density was assumed to remain constant, a liquid density of 998 kg/m^3 was determined [10] [11]. The liquid Reynolds numbers were calculated using Equation (15), and the gas Reynolds

numbers were calculated using Equation (16), as shown in column AD and column AE in Table 7. Again, the parameters for the gas Reynolds numbers had already been calculated, but some of the liquid Reynolds number parameters needed to be calculated. The dynamic viscosity was assumed to be constant at 22 C and equal to 9.532e-4 Pa-s [12] [13].

Table 7: An example of mass fluxes and Reynolds numbers. Notice that the liquid mass fluxes in column AA are the same because each set of experiments are run at the same liquid flow rate. Similarly, this explanation is why the liquid Reynolds numbers are the same in column AD. The 998 kg/m³ in column AA is not a liquid flux but instead the density used in the liquid calculations.

Z	AA	AB	AC	AD	AE
gas flux kg	liq flux kg/m2-s		u_L m/s	Re_L	Re_G
	998	kg/m3	2.47E-02		
0.36	24.62			77.49	60.02
0.32	24.62			77.49	52.00
0.21	24.62			77.49	35.12
0.12	24.62			77.49	20.07
0.12	24.62			77.49	20.04
0.09	24.62			77.49	15.07
0.05	24.62			77.49	8.84
0.04	24.62			77.49	6.08
0.00	24.62			77.49	0.00

Extrapolation

Because the pressure profile should decrease down the column, the calculated pressure drops should be positive. If they are not positive, either a standard flow pattern is not flowing through the column or the pressure transducers are not measuring the pressure correctly, meaning the data cannot be used for accurate calculations. For two experiments (Experiment 99 and Experiment 153), PT1-4 and PT2-4 had a negative pressure drop for the liquid only flow rate. Because the experimental data were not analyzed the same day the experiments were run, the experiments could not be rerun in the same pressure drop calibration conditions. Even though rerunning the experiments in new pressure drop calibration conditions should not cause a significant difference for analysis, the liquid only experiments are the basis for the X calculations, and the pressure drop calibration does introduce another possible error factor. As a result, it was decided to extrapolate the datum point, if possible. Before the point was extrapolated, similar, previous experiments that were run were compared to see how the pressure drop changed from G = 2.5 L/min to G = 0 L/min so that when the point was extrapolated, it could be evaluated whether the point seemed reasonable. Experiment 144, which had the same experimental

conditions, had a liquid only pressure drop of 1804 Pa while experiment 189 had a liquid only pressure drop of 960 Pa. As shown in Figure 16, the pressure drop versus the gas flow rate was plotted and fitted using Excel. Each best line of fit in Excel was tested. Usually, the polynomial best line of fit with a power up to 6 gave a positive intercept value with a coefficient of determination close to one. In the case of Figure 16, the polynomial to the sixth power gave a positive y intercept with an R^2 of 1.

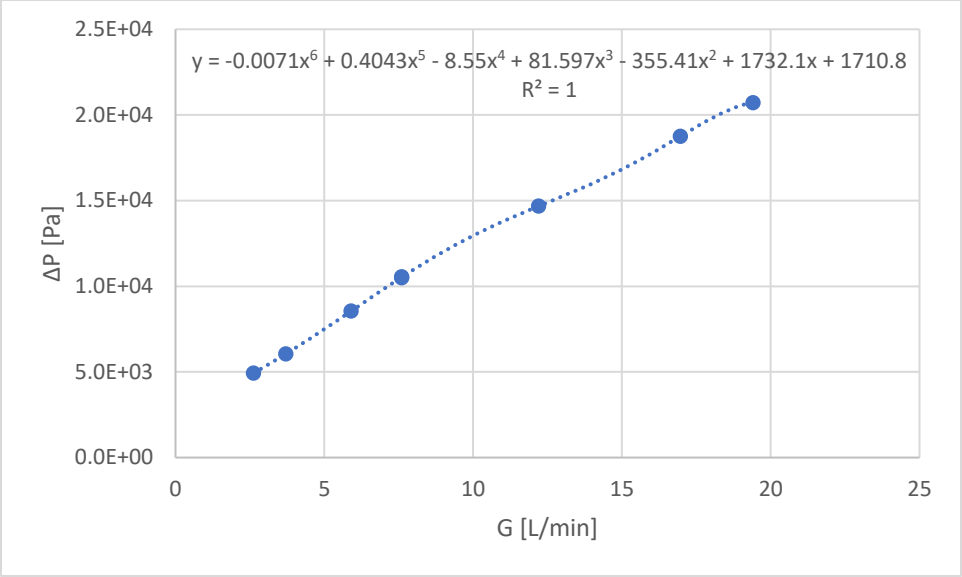

Figure 16: An example of an extrapolated point. For PT1-4, the G = 0 L/min point (y intercept) was extrapolated. The equation for the best line of fit and coefficient of determination are shown at the top of the figure.

The remaining extrapolation graphs can be found in the Extrapolation Curve section of Appendix D.

PT3

After running experiments and making figures like Figure 23, it was noticed that pressure drops using PT3 were consistently on or outside the 20% range when the other pressure transducers were within the 20% range. The other pressure transducers occasionally had experimental values near the 20% curve, but PT3 consistently had more values closer to the 20% curve than the calculated values, as shown in Figure 17. In addition, the previous user of the column mentioned past issues with PT3, especially fluids leaking at its connection to the column,

so glue held PT3 to the column, potentially causing error with its readings. Due to these past issues and current difficulties with PT3, PT3 was not used in calculations for this thesis.

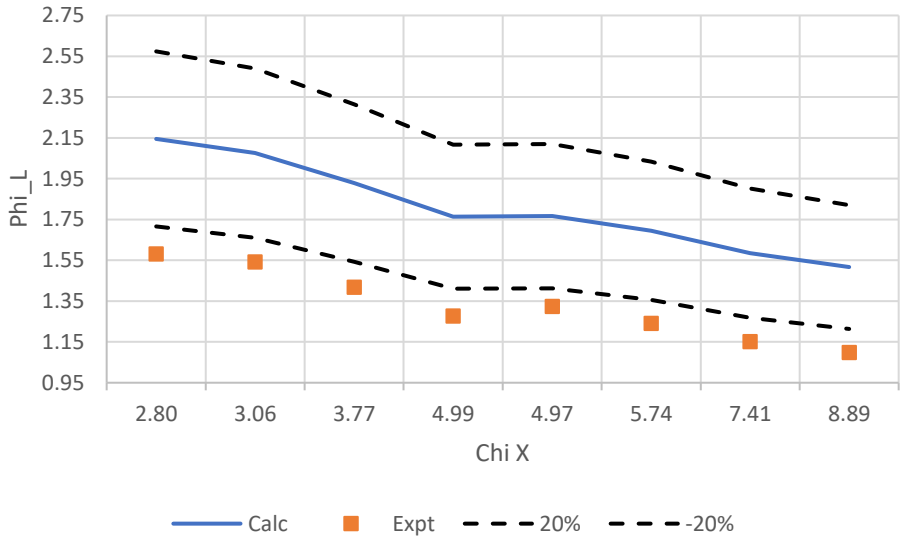

Figure 17: An example of a PT2-3 graph of Lockhart-Martinelli. Notice that the experimental values are outside the 20% calculated range. PT1-4 and PT2-4 were not outside the dashed lines for the same sets of experiments.

Packing

Originally, the packing stopped 1 inch below the distributor plate in the column. Experiments were run and the data was analyzed, but visually, distinguishing the flow patterns was difficult. Even though the distributor plate did its job of dispersing the air and water so that it could flow evenly throughout the column, the 1-inch gap allowed the water to redistribute to the center. As a result, entrance effects played a role in the experiments. To minimize the entrance effects, the 1-inch gap was filled with packing. After the gap was filled, the distributed air and water could not easily pool in the center of the column, resulting in more defined, visually identifiable flow patterns. All of the data analyzed in this thesis came from experiments run after the 1-inch gap was filled.

Wall effects add variables to empirical correlations, so in most laboratory settings, wall effects want to be kept to a minimum. Because the column has a 2-inch diameter, at least eight packing particles should fit along the diameter so that wall effects can be minimized [14]. Because of this restriction, 3-millimeter spheres were chosen as the packing size.

Flow Matrix

Based on the rotameters available and connected to the column, the flow matrix, shown in Figure 18, was used for the column. Each point on Figure 18 represents a gas and liquid flux in which the pressure trace for each pressure transducer was recorded. Because the liquid fluxes are two to three orders of magnitude larger than the gas fluxes, the flow is liquid dominated. Furthermore, each point has a defined or transitioning flow pattern.

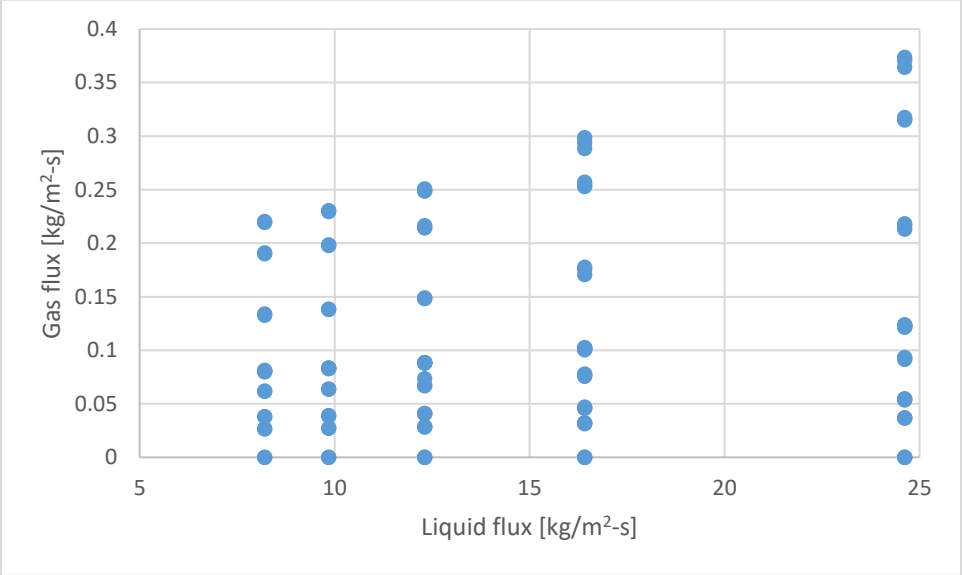

Figure 18: Flow matrix for the experiments.

The flow pattern can be determined visually or analytically. For these experiments, the visual flow pattern is shown in Figure 19, and the analytical flow pattern is shown in Figure 20. Looking at Figure 19, some of the transitions from pulse to bubbly flow happen in the trickle regime, which does not make sense. Visually identifying flow regimes can be difficult, especially at points of transition because one is relying on one's eyesight to differentiate differences.

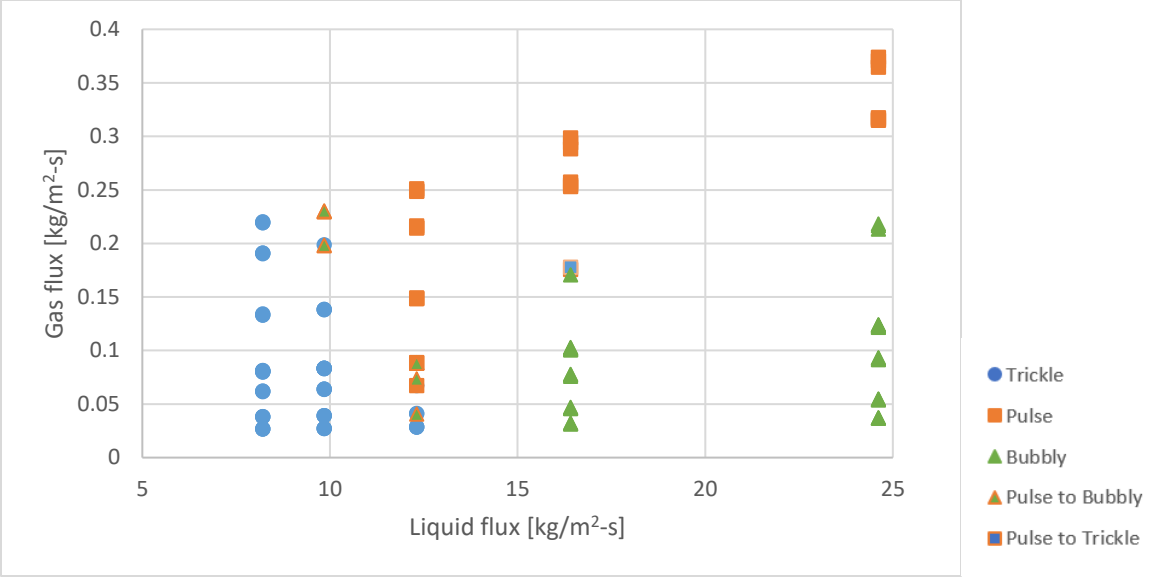

Figure 19: Visual flow pattern map.

Because visually determining the flow regimes is unreliable, an analytical method was used. PT4, the pressure transducer at the bottom of the column where the flow should be fully developed, had its pressure trace for each experiment graphs versus time. As explained in the Background section, the amplitude and relative pressure of the oscillations were compared to determine flow regime, as shown in Figure 20. (Sections of the graphs used for analysis are shown in the Pressure Trace for Analytical Flow Patterns section of Appendix D.) Looking at Figure 20, the transitions make more sense than the transitions shown in the visual flow patterns in Figure 19.

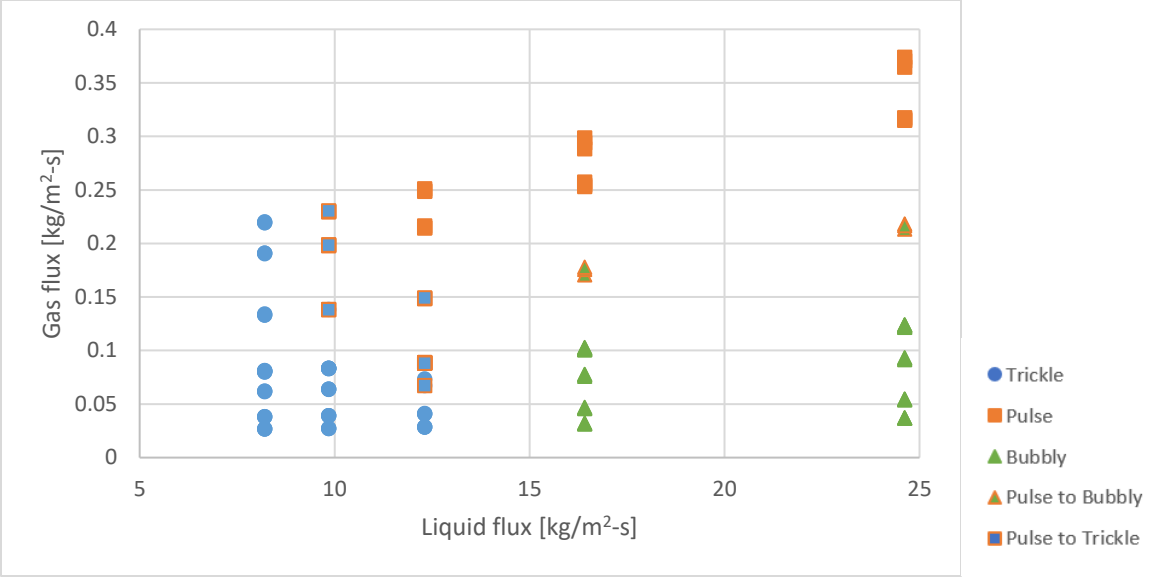

Figure 20: Analytical flow pattern map.

Using the analytical data, an estimation of each flow regime was marked, as shown in Figure 21.

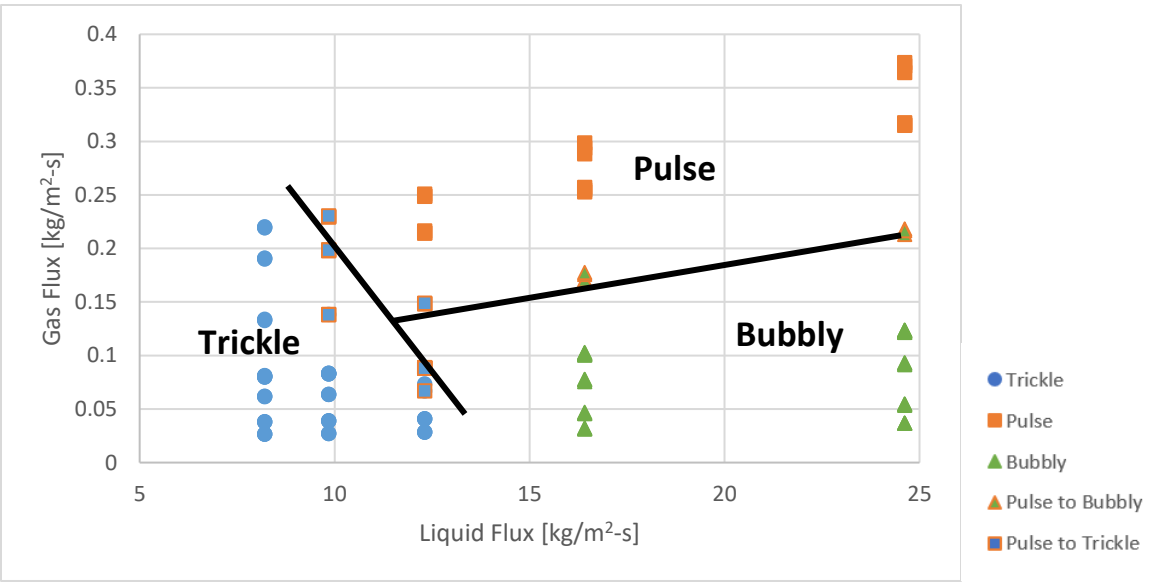

Figure 21: Analytical flow regime with transitions marked. The black lines mark estimated transitions between regimes.

Figure 21 can be compared to Figure 22, a well-known flow matrix from similar experiments done by reference [15], the Tosun flow map. Gas continuous is equivalent to trickle flow. Pulsing is pulse flow. Dispersed bubble and liquid continuous are equivalent to bubbly flow.

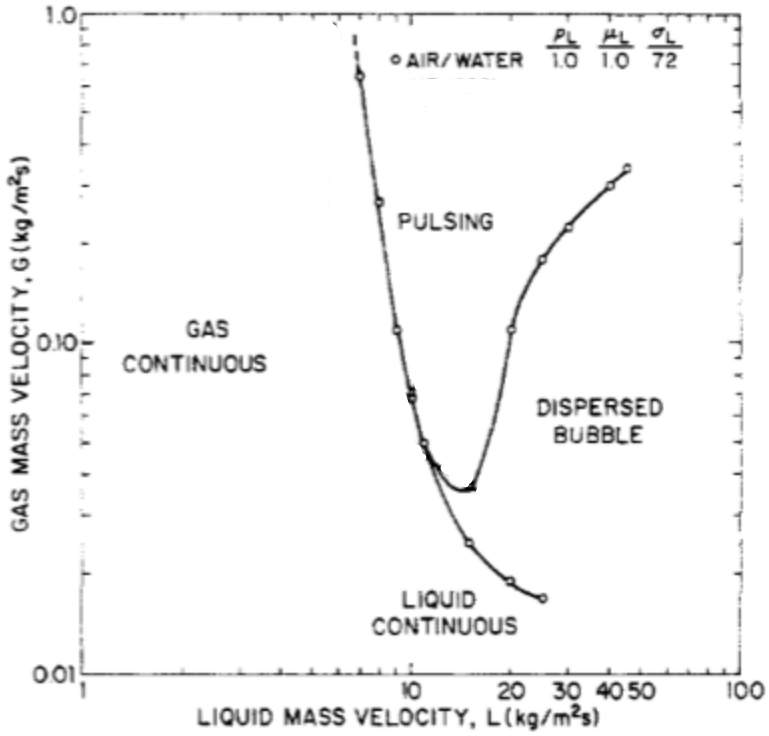

Figure 22: Flow regime map from reference [15]. The column has an inner diameter of 5.1 cm and a height of 91 cm. The beads have an average diameter of 1.9 mm.

Figure 22's bead size and column height are approximately 1.1 mm and 63.2 cm (respectively) smaller than Figure 21's bead size and column height. In Figure 22, the transition from pulse to bubbly flow happens at a lower G than in Figure 21, even though the liquid flux values are compatible. Even with these differences, the flow matrices are compatible considering the differences in experimental setup.

Lockhart-Martinelli Correlation

As explained in the Background section of the Introduction, the Lockhart-Martinelli correlation is an empirical method used to predict pressure drop in inertially dominated two-phase flow. It is not necessarily the best correlation to use to predict pressure drop in normal gravity (~9.8 m/s^2), but it is a starting point. As each set of experiments was analyzed in Excel, the experimental and calculated φ_L values were plotted against X, as shown in Figure 23, with the Lockhart-Martinelli correlation. In Figure 23, this set of experiments is less than 20% different from the theoretical values. These graphs were made for the pressure drops between PT1 and PT4 as well as for PT2 and PT4, respectively. The X values for the experimental and calculated or

theoretical values are the same. The focus of the graphs like Figure 23 is to compare the experimental φ_L to the calculated φ_L, to see how accurate each set of experiments is compared to calculated values.

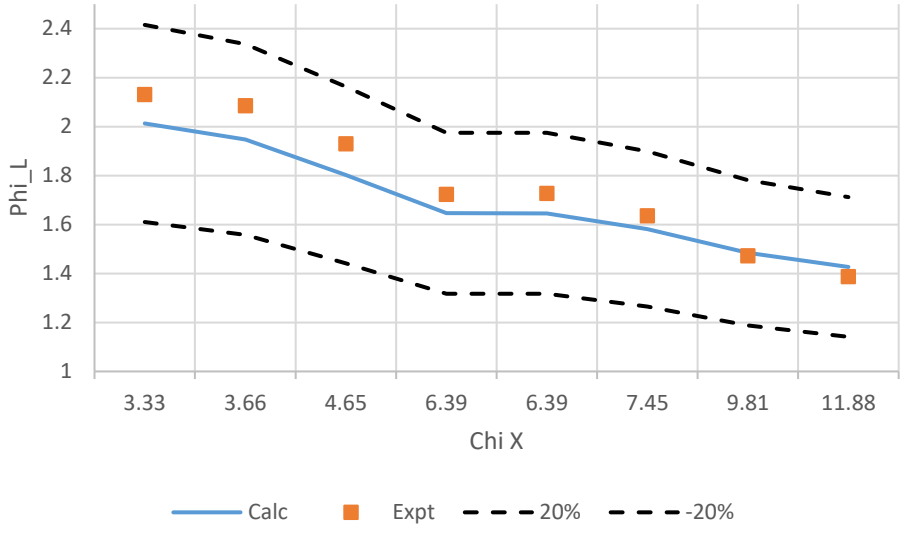

Figure 23: An example of a graphical representation of the Lockhart-Martinelli correlation. The orange squares (the experimental values) are less than 20% different from the center, blue (calculated values) line.

Looking at the individual sets of experiments is a good way to check that the experiments are running smoothly and accurately (to some degree), but looking at all of the experiments on a single graph gives a better overall view of the column.

Figure 24 shows the experimental data from all the sets of experiments of PT1-4 and PT2-4 plotted using Equations (1),(4), and (5). The data do not always stay within 20% of the calculated φ_L values, especially between X values one and five. When the experimental φ_L values are greater than the calculated φ_L values, either the two-phase gas-liquid pressure drop is higher than expected or the liquid-only pressure drop is lower than expected. Because the two-phase pressure drop has more parameters needed for analysis than liquid-only pressure drop and Lockhart-Martinelli is based on inertially dominated flows, the deviation most likely stems from the two-phase pressure drop having viscous or other frictional impacts increasing the pressure drop. However, the points that are near the calculated center line are inertially dominated flows.

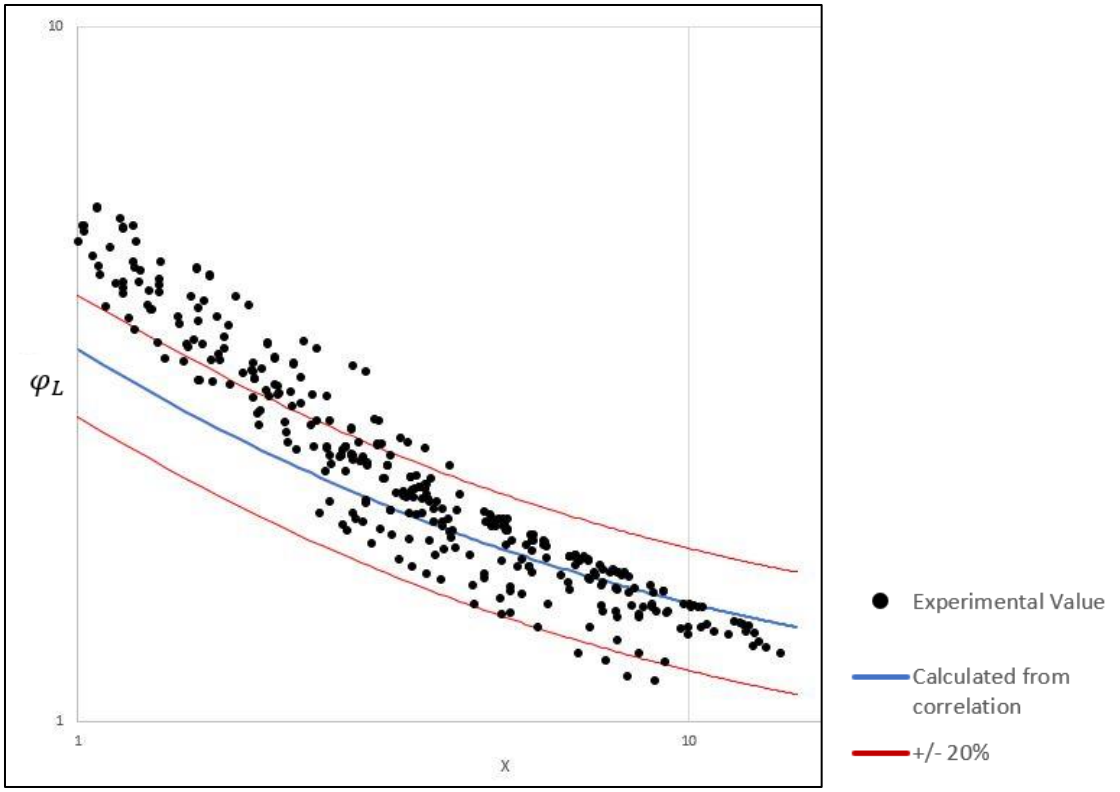

Figure 24: Experimental data compared to Lockhart-Martinelli correlation. [7] predicts +/- 14% of the data should fit between the two outer red lines; however, the data seems to be following a slightly different trend.

Because the Lockhart-Martinelli correlation has some constants in the correlation, the constants were adjusted to better fit the data, as shown in Figure 25. Equation (1) from reference [7] was changed to Equation (2), as shown by

$$\varphi_L = 1 + \frac{1}{X} + \frac{1.424}{X^{0.576}} \tag{1}$$

and

$$\varphi_L = 1.2 + \frac{2.3}{X} + \frac{1.9}{X^2} \ , \tag{2}$$

and even though the constants can be easily changed, the physical meaning of changing the constants is not straightforward [16]. Changing $\frac{1}{X}$ to $\frac{2.3}{X}$ could indicate that for X values of order unity, viscous effects are more dominate than the standard correlation predicted.

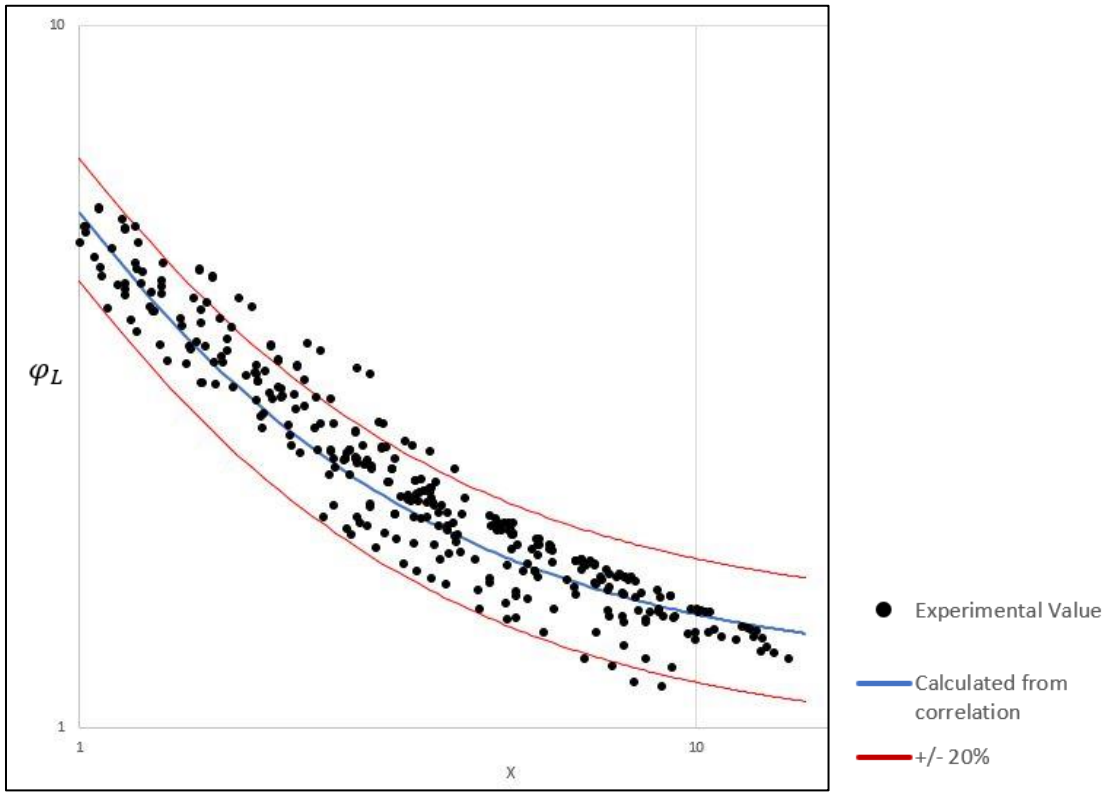

Figure 25: Experimental data compared to adjusted Lockhart-Martinelli.

Not all the data in Figure 25 fit within 20% (red lines) of the calculated values (center blue line), but changing the constants gives a better fit to the data. These changes show that the flow through the packed bed is not purely inertial and has other viscous or frictional interactions affecting its pressure drop, potentially transitioning as X values increase. Overall, the experimental data do not fully match the Lockhart-Martinelli correlation within 20%, but this discrepancy shows that the flow is not completely inertially dominated throughout the entire flow matrix.

Pressure Gradient Analysis

In general, the pressure is higher near the top of the column because the air and water are being mixed. Then, the air and water start developing a flow pattern, which allows both air and water to more easily flow through the column. As they flow through the column, the flow pattern further develops, which creates a pressure profile with decreasing pressure down the column. The pressure decreases because as the flow pattern develops, the air and water are more efficiently flowing down the column instead of colliding with each other. At higher flow rates, the air and water have more kinetic energy and friction when colliding with each other, creating a higher pressure drop throughout the column.

For analysis, usually the pressure drop normalized by length, or pressure gradient, is plotted against the changing liquid or gas parameter. Figure 26 is an example of this plot at a constant gas flux. The graph shows a nonlinear curve with distinct flow patterns as the liquid flux increases. Because each set of experiments run for this thesis were run at a constant liquid flux, graphs of the pressure gradient were plotted against gas flow rate and also Re_G. Reynolds number was chosen because it is a dimensionless parameter that compares viscous flow to turbulent flow, so a different perspective of analysis could be done, especially since the Lockhart-Martinelli correlation showed that the data was not always inertially dominated.

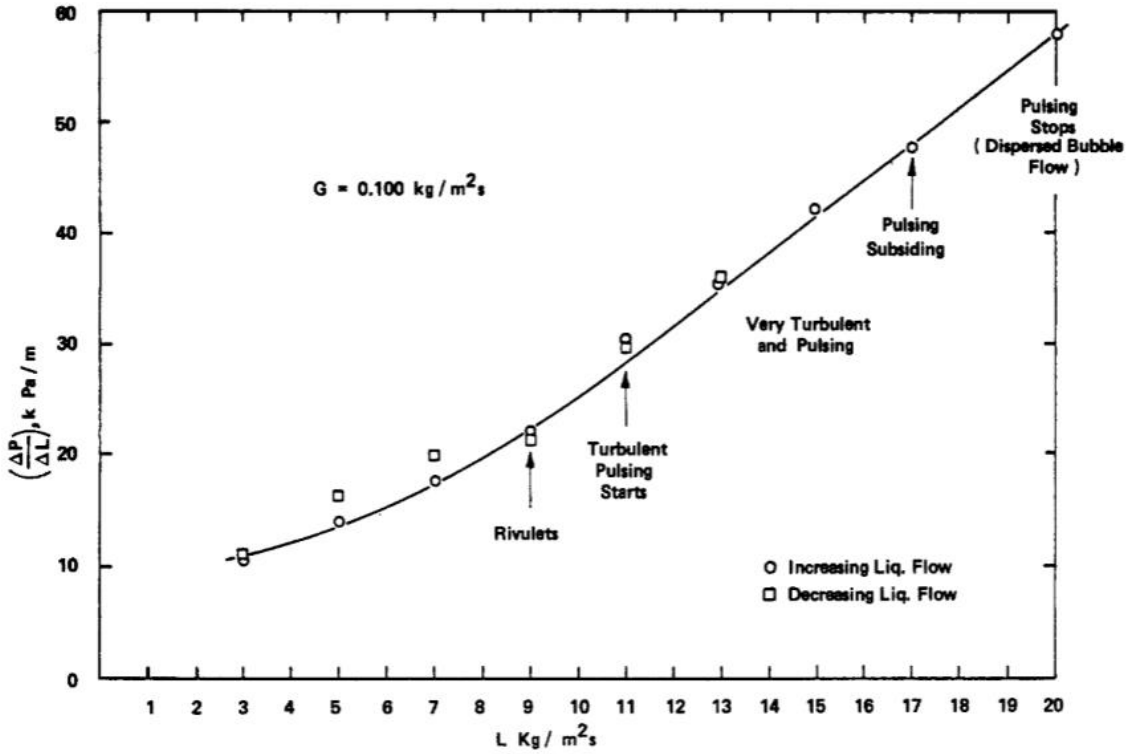

Figure 26: An example of pressure gradient versus liquid flux at a constant gas flux [7].

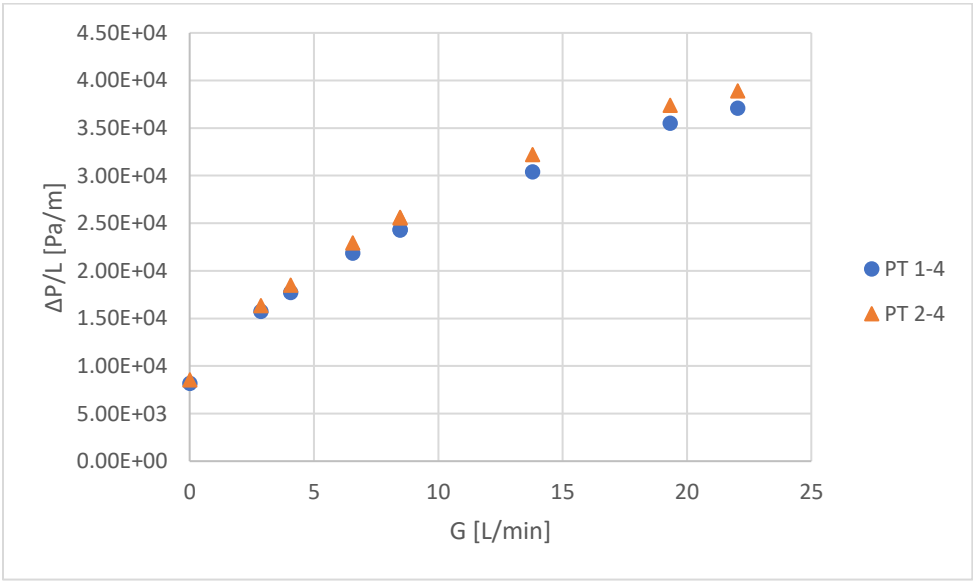

Figure 27: Pressure gradient versus gas flow rate for a set of experiments with a constant liquid flow rate of 3 L/min. Both the pressure gradients for PT1-4 and PT2-4 are shown.

Figure 27 shows the pressure gradients of PT1-4 and PT2-4 versus the gas flow rate. The points above 15 L/min are pulse flow, the points between 10 L/min and 15 L/min are transitioning flow, and the points less than 10 L/min are bubbly flow. (The points at a gas flow rate of 0 L/min is a liquid-only pressure drop.) At higher gas flow rates, the pressure drop is higher, which makes sense because there is more friction in the column. Both Figure 26 and Figure 27 show a nonlinear, continuous curve, each with opposite concavity because they plot a different x-axis, but neither has any visual indicators that the flow pattern is changing. Figure 27 does have some gaps or spacing between the transition point and the defined flow patterns, but this spacing could be coincidental to the test matrix. When the flow pattern is transitioning from pulse to trickle, as shown in Figure 28, there is also not a visual indicator, and the spacing between the data points is arbitrary to the flow pattern. The points above a gas flow rate of 15 L/min are pulse flow, the points at approximately 12 L/min and 7 L/min are transitioning from pulse to trickle, and the points below 7 L/min are trickle flow. (The points at a gas flow rate of 0 L/min are a liquid-only pressure drop.) Since a packed column can be optimized with flow pattern and pressure drop, a helpful graph for operators would be one that can easily show both parameters. This common method of pressure gradient analysis is not helpful for visually determining flow patterns or transitions unless the flow patterns are marked on the figure (like with Figure 26), which is unrealistic to do in the chemical industry. Overall, these figures would not help an operator easily optimize a packed column.

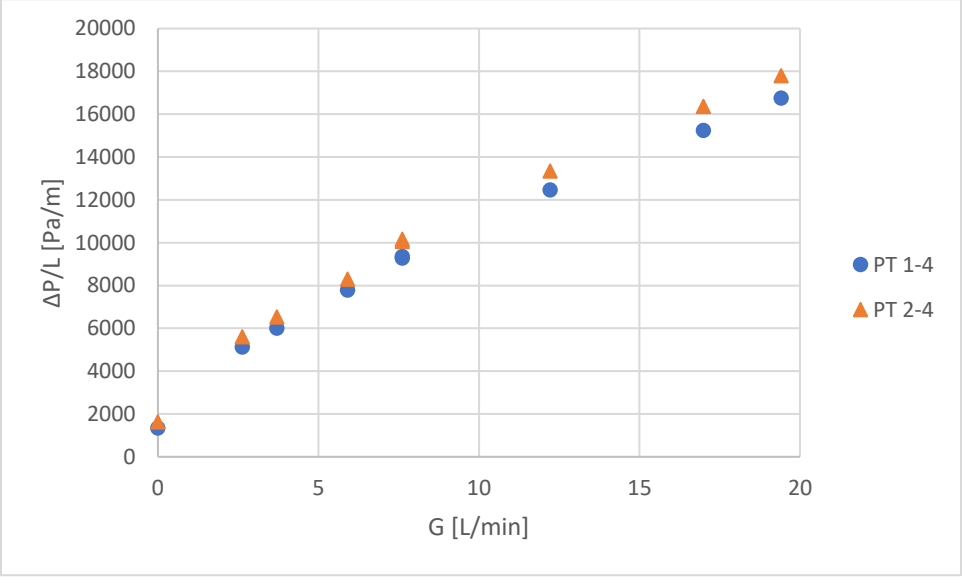

Figure 28: Pressure gradient versus gas flow rate for a set of experiments with a constant liquid flow rate of 1.5 L/min. Both the pressure gradients for PT1-4 and PT2-4 are shown.

Instead of using flow rate or flux as the x-axis, the next pressure gradient analysis used Re_G. In Figure 29, the sets of experiments greater than a Re_G of 50 are pulse flow while the sets of experiments less than a Re_G of 10 are bubbly flow. The points in-between are transitioning flow from pulse to bubbly. In Figure 30, the Re_G values greater than 30 are pulse flow, the Re_G values less than approximately 10 are trickle flow (where experiment 231 was determined to be a transition flow), and the points in-between were determined to be flows transitioning from pulse to trickle. Both Figure 29 and Figure 30 produce nonlinear curves, but again there is not a visual indicator of flow pattern with this pressure gradient graph. This pressure gradient analysis shows that at approximately viscous flows, the pressure drop increases with an increasing Re_G value, but an operator probably would not know how to use this information. The remaining figures can be found in the Pressure Gradient Graphs section of Appendix D.

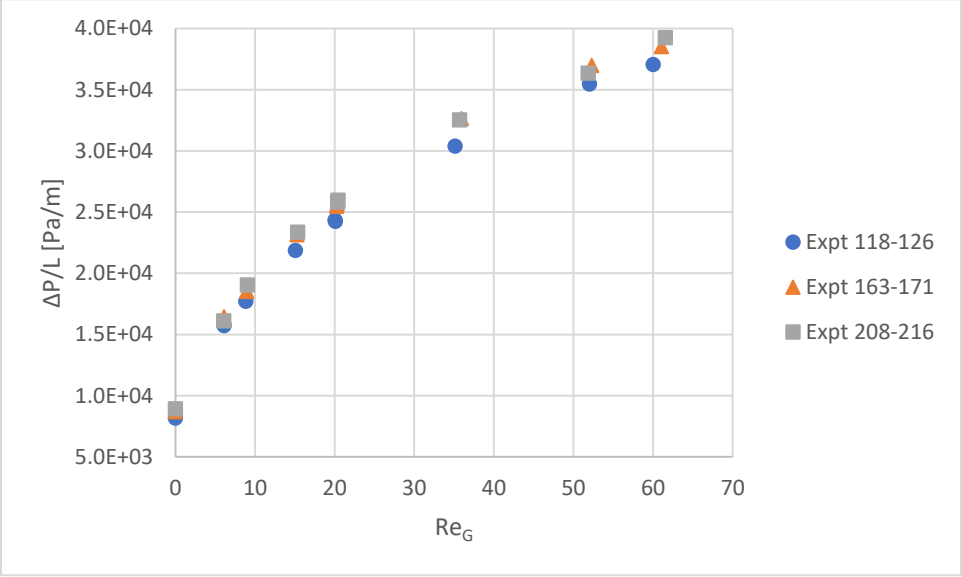

Figure 29: Pressure gradient of PT1-4 versus Re_G. The liquid rate was held constant at 3 L/min (Re_L = 77.49). The flow transitioned from pulse to bubbly.

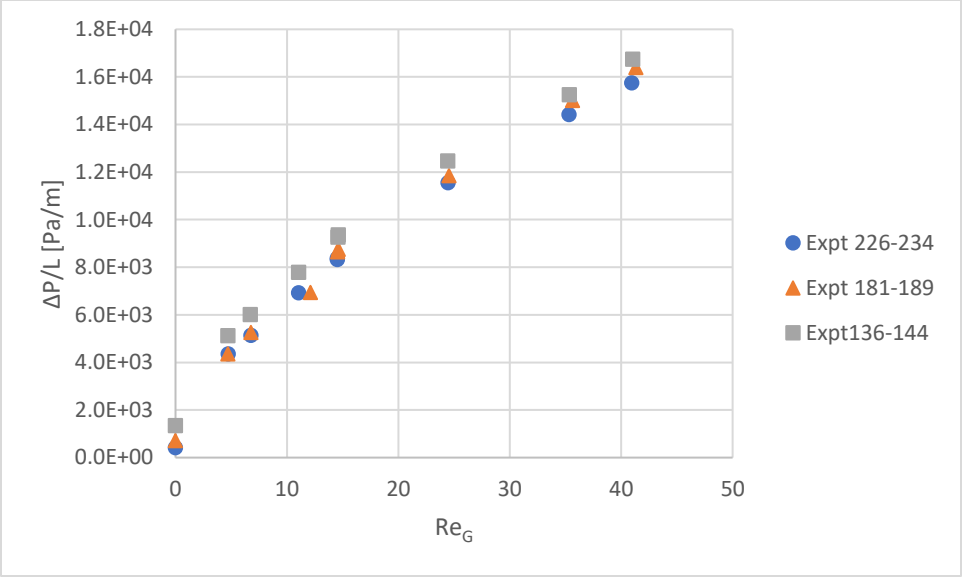

Figure 30: Pressure gradient of PT1-4 versus Re_G. The liquid rate was held constant at 1.5 L/min (Re_L=38.74). The flow transitioned from pulse to trickle.

Standard Deviation/Average Versus Gas Flow Rate Analysis

In industry, it is more common to see a flow gauge with units (like L/min) instead of a dimensionless parameter like Re or flux values (which need to know changing chemical properties). Also, following a pressure profile and dividing by an average is relatively easy, so overall, this type of analysis is easily found or calculated with common industry measurements. When the change in pressure was evaluated this way, transition of flow was shown visually with a change in slope. Note, graphically, a set of data is considered a triangle, circle, and square for approximately the same gas flow rate.

In Figure 31, as the gas flow rate increases, the standard deviation of PT4 normalized by its average increases nonlinearly. At the gas flow rates greater than 15 L/min, the data points were analytically determined to be pulse flow. At the gas flow rates less than 10 L/min, the data points were analytically determined to be bubbly flow. The data points between 10 L/min and 15 L/min was analytically determined to be in transition. If a straight line was drawn from the bubbly points through the transition, this line would not intersect the points considered pulse. If a straight line was drawn from the pulse flow to the transition, this line also would not intersect the bubbly points. The transition in flow appears to be visually indicated by a change in slope between the bubbly and pulse flow. Figure 32 demonstrates this idea with hand placed lines on the graph. The lines are not the analytical slopes of the points, and more analytical analysis should be done

to further prove this idea valid. However, visually, this idea of the transition flow regime being the change of slope seems valid at a liquid flow rate of 3 L/min with the flow pattern changing from pulse to bubbly flow.

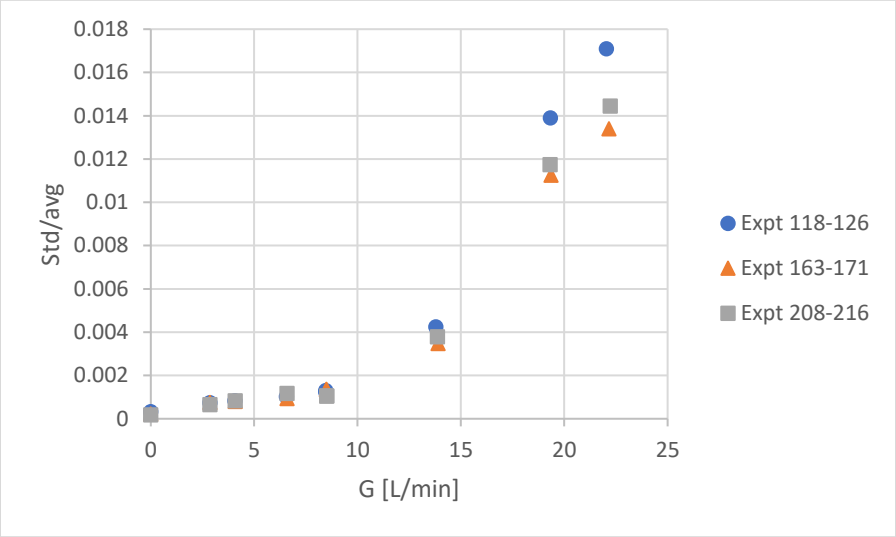

Figure 31: Standard deviation of PT4 normalized by its average versus gas flow rate. The liquid flow rate was held constant at 3 L/min.

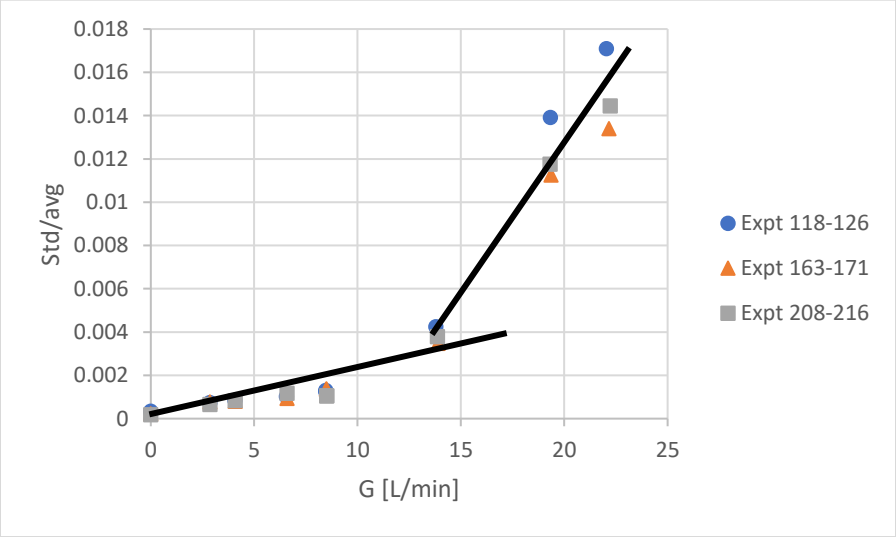

Figure 32: Visually drawn lines to demonstrate change in slope of Figure 31. These lines are not the analytical slopes.

In Figure 33, as the gas flow rate increases, the standard deviation of PT4 normalized by its average increases nonlinearly. Like in Figure 31, the transition region are the points between 10 L/min and 15 L/min, the bubbly regime is the points less than 10 L/min, and the pulse regime

are the points above 15 L/min. If a straight line is drawn from the bubbly flow to the transition point, this line would have a different slope to a line drawn from the pulse flow to the transition point, as shown in Figure 34. Though more analytical analysis needs to be done, visually, the transition between bubbly and pulse flow at a liquid flow rate of 2 L/min again is shown with a change in slope.

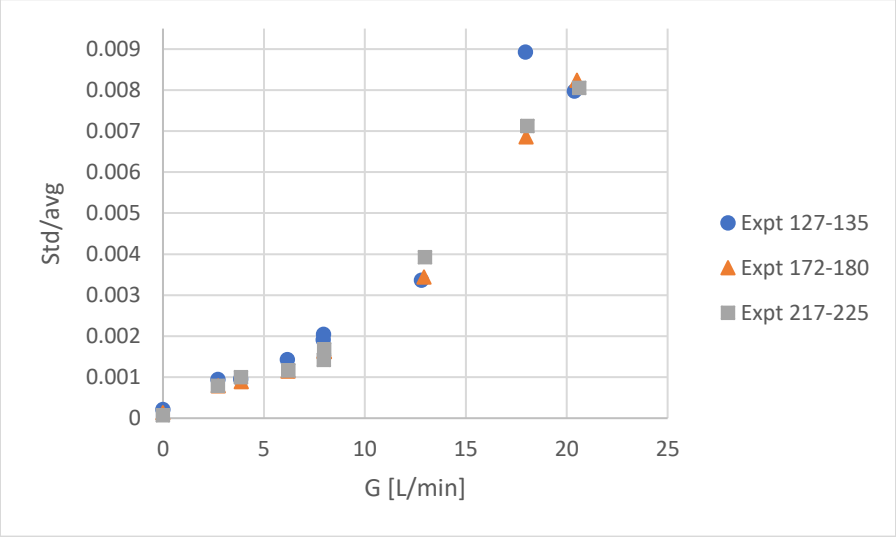

Figure 33: Standard deviation of PT4 normalized by its average versus gas flow rate. The liquid flow rate was held constant at 2 L/min.

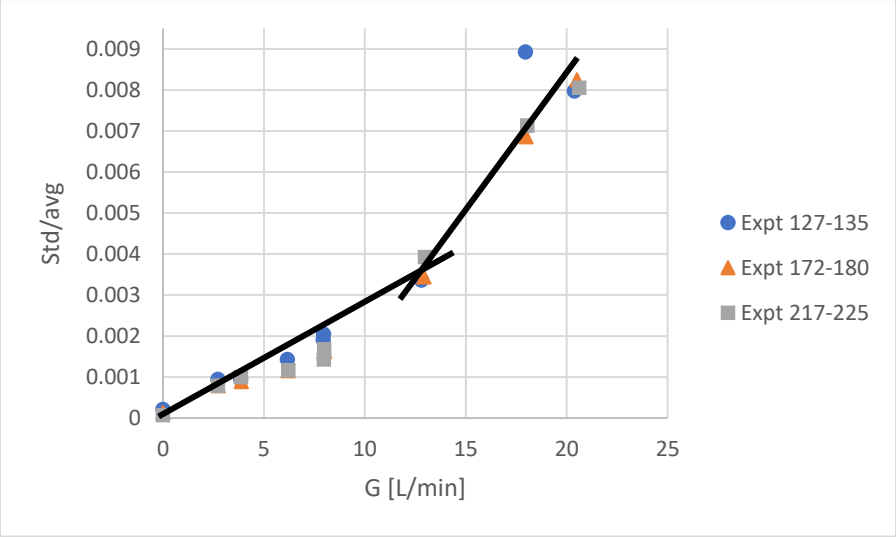

Figure 34: Visually drawn lines to demonstrate change in slope of Figure 33. These lines are not the analytical slopes.

In Figure 35, visually, as the gas flow rate increases, the standard deviation of PT4 normalized by its average increases more linearly than Figure 31 or Figure 33. The transition region in Figure 35 includes more points, and the analytical analysis was less defined on where the transition region is when comparing repetitions. The first two sets of data points (less than 5 L/min) were considered trickle flow. The last two sets of data points (greater than 15 L/min) were considered pulse flow. The data points in-between were analytically considered transition, or one of the experiments in a set had a defined flow regime while the other two experiments defined the regime as transition. Even with a less defined flow regime, if a straight line is drawn from the trickle flow to the transition, it will not intersect all the points in the pulse region, as shown in Figure 36. Furthermore, the transition region appears to have a different slope than the defined regions. Even though the lines in Figure 36 are not the analytical slopes, they do show that at least visually, there is a change in slope in the transition region from pulse to trickle flow at a liquid flow rate of 1.5 L/min., and the transition region itself appears to have its own slope.

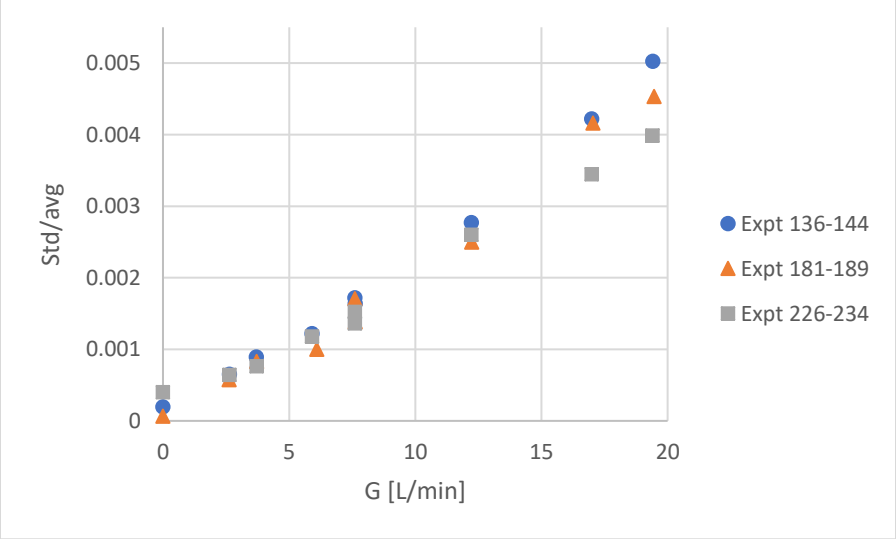

Figure 35: Standard deviation of PT4 normalized by its average versus gas flow rate. The liquid flow rate was held constant at 1.5 L/min.

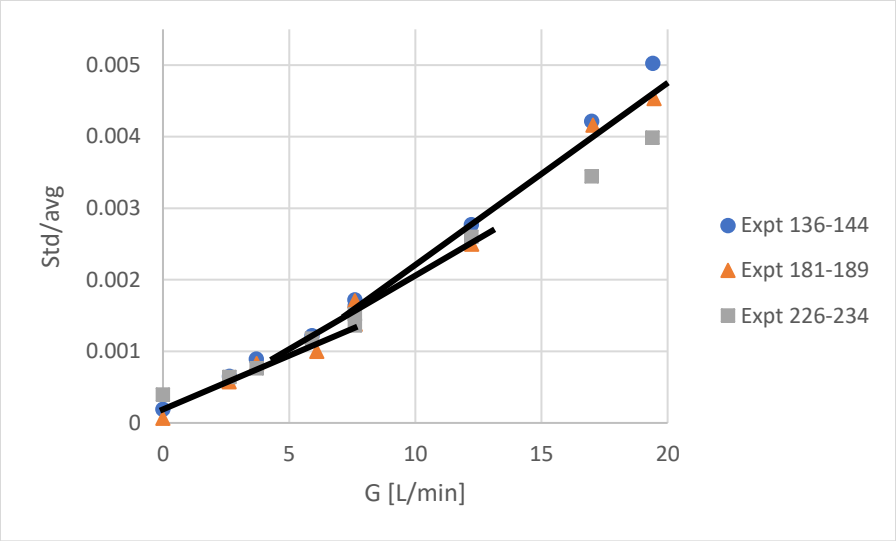

Figure 36: Visually drawn lines to demonstrate change in slope of Figure 35. These lines are not the analytical slopes.

In Figure 37, as the gas flow rate increases, the standard deviation of PT4 normalized by its average increases nonlinearly. All the data sets (except the orange triangle between 10 L/min and 15 L/min) greater than 10 L/min were analytically determined to be transition flow. The remaining data points below 10 L/min were determined to be trickle flow. Visually, there is a change in slope from the transition region to the trickle region, as shown in Figure 38. Even though Figure 38 only shows the transition region to the trickle region, there is still a visual change in slope between the two regions at a liquid flow rate of 1.2 L/min.

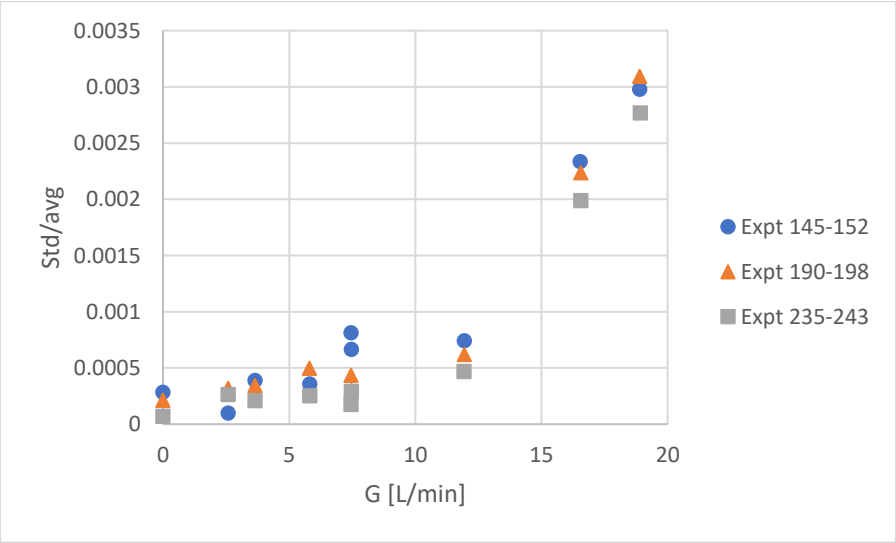

Figure 37: Standard deviation of PT4 normalized by its average versus gas flow rate. The liquid flow rate was held constant at 1.2 L/min.

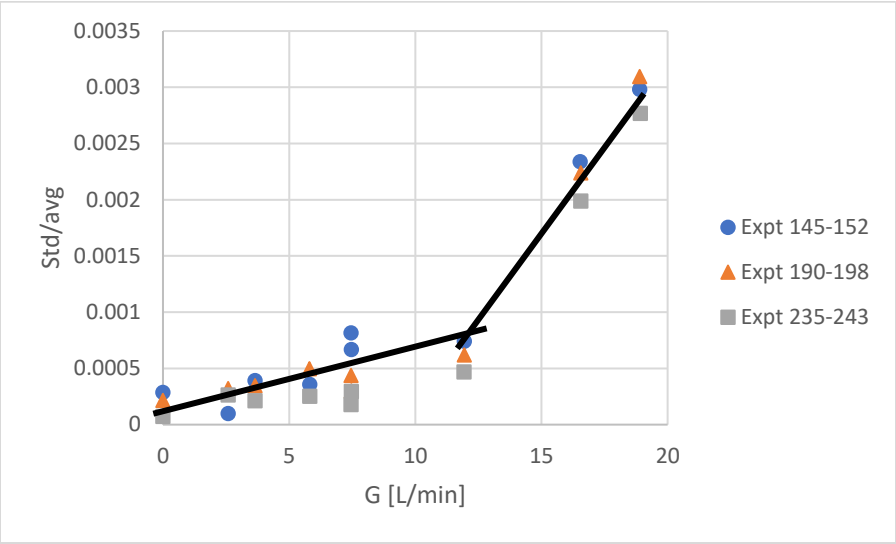

Figure 38: Visually drawn lines to demonstrate change in slope of Figure 37. These lines are not the analytical slopes.

In Figure 39, there is no transition point; the flow is only trickle. There does not appear to be a visual identifiable slope. Furthermore, the y-axis has a such a narrow range that if zoomed out, the points would appear to have a horizontal, straight line. With no visual change in slope, there should not be a transition point according to the analysis, and there is not.

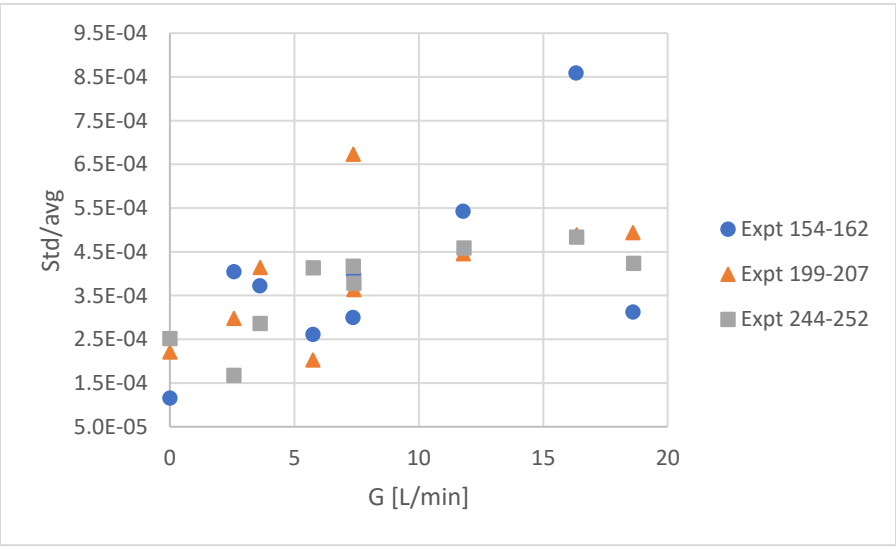

Figure 39: Standard deviation of PT4 normalized by its average versus gas flow rate. The liquid flow rate was held constant at 1 L/min.

Reference [17] plots data in a similar manner in Figure 40. The standard deviation is not normalized by its average, but the concept is similar. The flow patterns for these data are not listed, but each respective liquid flux creates a nonlinear curve as the gas flux increases. If the flow patterns are known, this analysis method could be evaluated with microgravity compared to normal gravity to see if changing other parameters still renders the visual analysis valid.

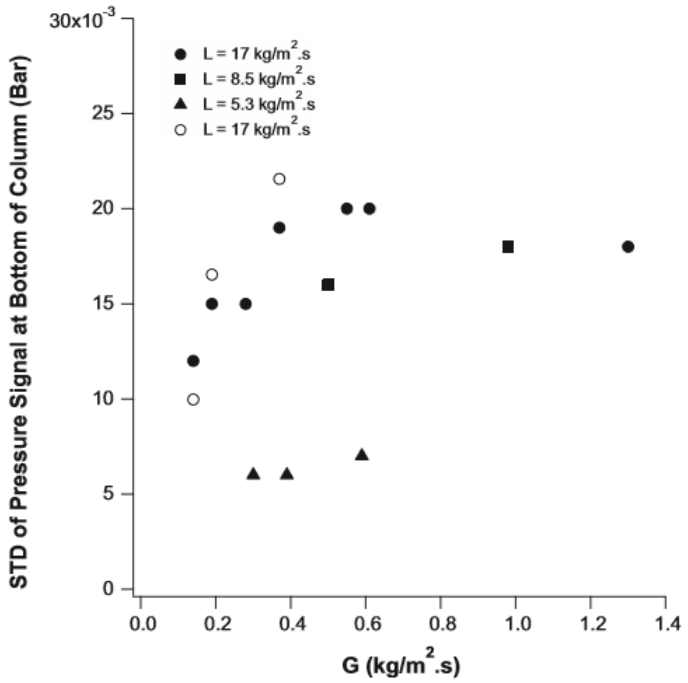

Figure 40: Pressure data in both microgravity (0g) and normal gravity (1g) from [17]. The open symbols represent normal gravity while the solid symbols represent microgravity.

Overall, this analysis seems helpful for operators optimizing packed columns. Even though the change in pressure is evaluated in an unusual way, a change in flow pattern can be shown visually with a change in slope, which is an identifier for operators trying to optimize a packed column. Compared to the standard pressure gradient analysis and flow maps, the standard deviation evaluation method allows both change in flow pattern and change in pressure to be evaluated on one graph. This analysis uses parameters easily found in a chemical plant, but a more analytical evaluation should be completed to verify the results.

4. Summary and Conclusions

Packed bed columns are widely used throughout many chemical, petrochemical, and biochemical processes to carry out reactions between solid catalysts and gas-liquid reactants. A common type of setup for these reactors is downward, cocurrent flow, as was modeled with this thesis. Flow patterns and their associated pressure drops are two important parameters that can optimize the operation of these reactors. However, the analysis of these parameters is usually above the understanding of the operators who control the reactors. This thesis evaluates these two parameters in a laboratory scale packed bed column, compares the results to literature values, and analyzes the data in a simpler way using parameters easily found with plant or lab equipment/sensors.

After the raw data was analyzed in Excel to calculate the necessary parameters, it was compared to the well-known Tosun flow map and the Lockhart-Martinelli correlation. Even though the Tosun flow map was based on experiments with a different sized column and packing, the analytically-determined experimental flow map from this thesis was compatible to the Tosun flow map, showing that the flow patterns determined were reasonable. When the data were plotted with the Lockhart-Martinelli correlation and parameters, not all the data fit within 20% of the expected values. This discrepancy could come from the fact that the flow is not inertially dominated throughout the entire flow matrix. Adjustments were made to the Lockhart-Martinelli correlation constants, which gave a better fit to the trend. Overall, the experiments seemed consistent with literature values.

When analyzing a pressure drop curve, whether it is plotted against gas or liquid flow rate or mass flux or Reynolds number, the change in flow pattern cannot be seen visually. However, when the pressure was analyzed as a pressure trace standard deviation normalized by its average versus its gas flow rate, the data had a visual change in slope whenever the flow pattern transitioned. This visual analysis allows operators to easily identify when the flow pattern and pressure inside the packed column are changing, respectively, so that they can reoptimize the column.

Multivariable analysis should be tested to see how changing different variables affects the change in slope to see if the experiments are biased, since only one variable, the gas flow rate, changed. Overall, with water and air flowing concurrently downward, at approximately constant temperature, this visual analysis (graphing the pressure trace standard deviation normalized by it

average versus its gas flow rate) indicates an easier way to show changes in flow pattern and pressure with parameters easily found in a chemical plant.

Recommendations for Further Research

Because this thesis only ran experiments with air and water in a packed bed with uniform spheres, a recommendation to see if the standard deviation analysis works for other scenarios would be to change possibly bias parameters. Changing the viscosity of the fluid, the temperature, gravity, wetting, and the test matrix to include both increasing and decreasing flow rates would see if multivariable changes impacted the visual analysis. Changing the packing to Rachig rings, textured beads, or catalyst would be more realistic to the industry and would see if packing affects the visual analysis. Finally, analytically determining the slopes (and their respective margin of errors) between transition points and defined regimes will further validate or deny the visual analysis.

References

[1] G. Graham, P. Pednekar and D. Bunning , "Distillation, Part -1 : Experimental Validation of Column Simulations," *Chemical Engineering,* pp. 30-37, 1 Feb 2018.

[2] J. Shiny and Y. G. B. Varma , "Flow pattern and pressure drop in gas-liquid in cocurrent downflow through packed beds," *Bioprocess Engineering,* vol. 12, pp. 215-220, 1995.

[3] B. Motil, Gas-Liquid Two-Phase Flow Through Packed Bed Reactors In Microgravity, Ph.D Dissertation, Cleveland: Case Western Reserve University, 2006.

[4] T. Zhao, T. Eda, S. Achyut, J. Haruta, M. Nishio and M. Takei, "Investigation of pulsing flow regime transition and pulse characteristics in trickle-bed reactor by electrical resistance tomography," *Elsevier,* vol. 130, pp. 8-17, 2015.

[5] E. Ozahi, M. Y. Gundogdu and M. Ö. Carpinliogl, "A Modification on Ergun's Correlation for Use in Cylindrical," *Advanced Powder Technology,* p. 369–381, 2008.

[6] R. W. Lockhart and R. C. Martinelli, "Proposed Correlation Of Data For Isothermal Two-Phase, Two-Component Flow In Pipes," *Chemical Engineering Progress,* vol. 45, no. 1, pp. 39-48, 1949.

[7] G. Tosun, "A Study of Cocurrent Downflow of Nonfoaming Gas-Liquid Systems in a Packed Bed. 2. Pressure Drop: Search for a Correlation," *Ind. Eng. Chem. Process Des. Dev.,* vol. 23, no. 1, pp. 35-9, 1984.

[8] J. D. Seader, E. J. Henley and D. K. Roper, "6.1.2 Packed Columns," in *Separation Process Principles*, Hoboken, Wiley, 2016, pp. 140-3.

[9] M. J. McCready, B. J. Motil and V. Balakotaiah, "FUNDAMENTAL STUDIES ON TWO-PHASE GAS-LIQUID FLOWS THROUGH PACKED BEDS IN MICROGRAVITY," *NASA,* pp. 265-75, 2002.

[10] Engineering Toolbox, "Water - Density, Specific Weight and Thermal Expansion Coefficient," Engineering Toolbox, 2003. https://www.engineeringtoolbox.com/water-density-specific-weight-d_595.html.

[11] USGS, "Water Density," USGS, 9 Apr 2018. https://water.usgs.gov/edu/density.html.

[12] Engineering Toolbox, "Water - Dynamic and Kinematic Viscosity," Engineering Toolbox, 2004. https://www.engineeringtoolbox.com/water-dynamic-kinematic-viscosity-d_596.html?vA=22&units=C#.

[13] Engineers Edge LLC, "Water - Density Viscosity Specific Weight," Engineers Edge LLC. https://www.engineersedge.com/physics/water__density_viscosity_specific_weight_13146.htm.

[14] V. G. Rao and A. A. H. Drinkenburg, "A Model for Pressure Drop in Two-Phase Gas-Liquid Downflow Through Packed Columns," *AIChE Journal,* vol. 31, no. 6, pp. 1010-1018, 1985.

[15] G. Tosun, "A Study of Cocurrent Downflow of Nonfoaming Gas-Liquid Systems in a Packed Bed. 1. Flow Regimes: Search for a Generalized Flow Map," *Ind. Eng. Chem. Process Des. Dev,* vol. 23, no. 1, pp. 29-34, 1984.

[16] D. Chisholm , "A THEORETICAL BASIS FOR THE LOCKHART-MARTINELLI CORRELATION FOR TWO-PHASE FLOW," *lnr J Heat Moss Transfer ,* vol. 10, pp. 1767-78, 1967.

[17] P. Salgi, V. Balakotaiah, E. Rame and B. Motil, "Pulse properties in gas–liquid flow through randomly packed beds under microgravity conditions," *International Journal of Multiphase Flow,* vol. 73, pp. 11-16, 2015.

[18] The Engineering Toolbox, "Air - Dynamic and Kinematic Viscosity," The Engineering Toolbox, 2003. https://www.engineeringtoolbox.com/air-absolute-kinematic-viscosity-d_601.html?vA=22&units=C#.

[19] Engineers Edge, "Viscosity of Air, Dynamic and Kinematic," Engineers Edge LLC. https://www.engineersedge.com/physics/viscosity_of_air_dynamic_and_kinematic_14483.htm.

[20] S. Ergun, *Chem. Eng. Prog.,* vol. 48, no. 2, p. 89, 1952.

[21] C. E. Brennen, "Flow Patterns," in *Fundamentals of Multiphase Flows*, Cambridge University Press, 2005, pp. 163-195.

5. Appendices

Appendix A

The Ergun equation used to calculate the gas-only pressure drop was

$$\frac{(-\Delta P)}{L} = \frac{C_1 \mu (1-\varepsilon)^2 u}{\varepsilon^3 d_p^2} + \frac{C_2 (1-\varepsilon) \rho u^2}{\varepsilon^3 d_p}, \tag{3}$$

where the parameters had the following values: μ = 1.82 e -5 Pa-s [18] [19], d_p = 3mm, C_1 = 118.2, and C_2 = 1.0. Equation (3) came from reference [20]. The ρ_{air} and ε were calculated using Equation (6) and (7). When only one phase is flowing through a packed column, friction is the main force contributing to the pressure drop. The Ergun equation is derived from a friction factor and a modified Re, which can be rearranged to get the inertial and viscous terms shown in Equation (3).

Appendix B

Equation (1) is the Lockhart-Martinelli correlation determining φ_L while Equation (2) is the adjusted Lockhart-Martinelli correlation used to better fit the experimental data. The equations are shown in the Lockhart-Martinelli Correlation section. The following equations use experimental parameters to calculate Lockhart-Martinelli parameters from reference [7]:

$$X = \sqrt{\frac{\frac{\Delta P}{L}_L}{\frac{\Delta P}{L}_G}}, \tag{4}$$

$$\varphi_L = \sqrt{\frac{\frac{\Delta P}{L}_{LG}}{\frac{\Delta P}{L}_L}}. \tag{5}$$

Appendix C

The following equations were used to calculate the properties and parameters of the packed column. Equation (6),

$$\rho_{air} = \frac{P}{RT}, \tag{6}$$

calculated the air density in the column, and Equation (*7*),

$$\varepsilon = \frac{V_{col} - V_{bead}}{V_{col}}, \tag{7}$$

calculated the bed porosity in the column where V_{col} and V_{bead} are

$$V_{col} = \pi \frac{D^2}{4} H_{col} \tag{8}$$

and

$$V_{bead} = \frac{m_{bead}}{\rho_{bead}} \tag{9}$$

respectively. Ideal gas was chosen because the temperature was relatively high, and the pressure was relatively low.

Equation (10),

$$u = \frac{(Flux)}{\rho} = \frac{volumetric\ flux}{A}, \tag{10}$$

is the superficial velocity of the gas or liquid, and if the equation is rearranged, it can become the mass flux of the liquid or gas, as shown by

$$L_{flux} = u_L \rho_L \tag{11}$$

and

$$G_{flux} = u_G \rho_G . \tag{12}$$

The rotameters for the gas-side of the system required a correction factor, as shown by

$$K_G = \sqrt{G \frac{T_{act}}{T_o} \frac{P_o}{P_{act}}}. \tag{13}$$

The correction factor was then used to correct the experimental gas flow rate, as shown by

$$Q_G = \frac{Q_{air}}{K_G}. \tag{14}$$

The parameter Q_{air} is the gas flow rate value read straight from the gas rotameter.

The Reynolds number for the liquid and gas were calculated using

$$Re_L = \frac{\rho_L u_L d_p}{\mu_L}, \tag{15}$$

where μ_L= .0009532 Pa-s and ρ_L = 998 kg/m^3 , and

$$Re_G = \frac{\rho_G u_G d_p}{\mu_G}. \tag{16}$$

The gas parameters were previous calculated with Equation (6) and (10).

Appendix D

Pressure Trace for Analytical Flow Patterns

On each figure, each experiment was compared to each other to analytically determine the flow pattern. Figure 41, Figure 42, Figure 43, Figure 44, Figure 45, Figure 46, Figure 47, Figure 48, Figure 49, Figure 50, Figure 51, and Figure 52 show sections of the pressure traces for each set of experiments.

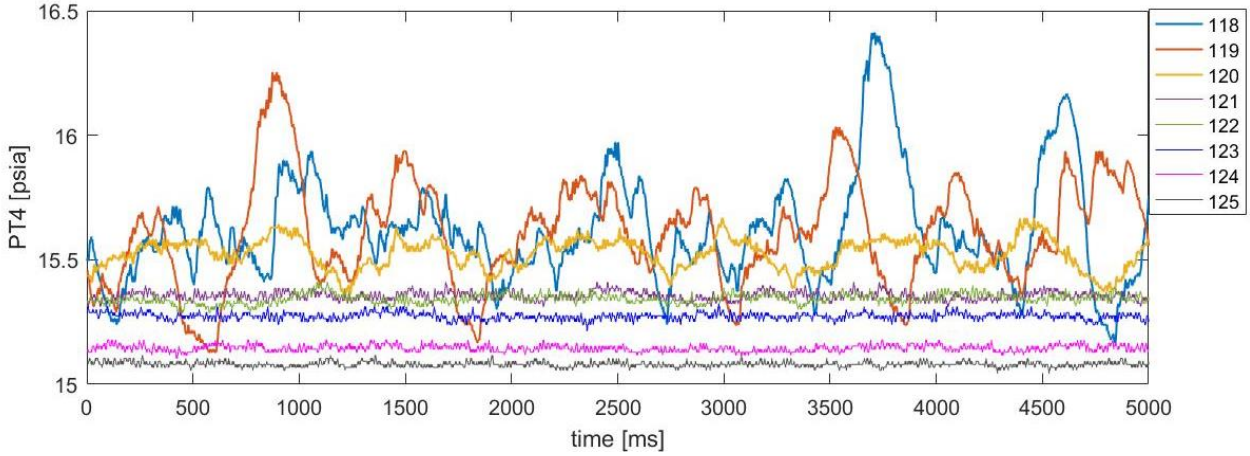

Figure 41: Section of the pressure traces for experiments 118-125.

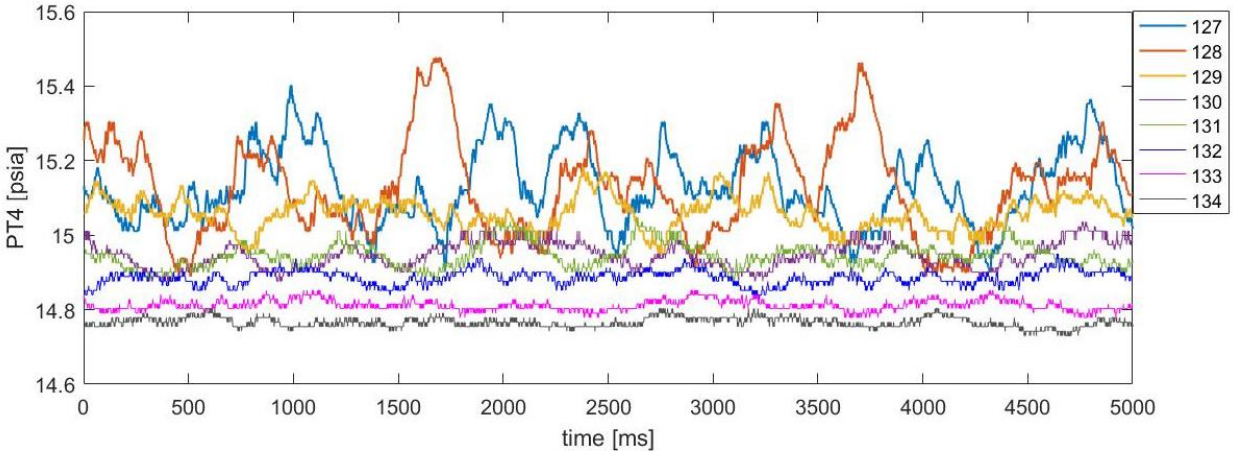

Figure 42: Section of the pressure traces for experiments 127-134.

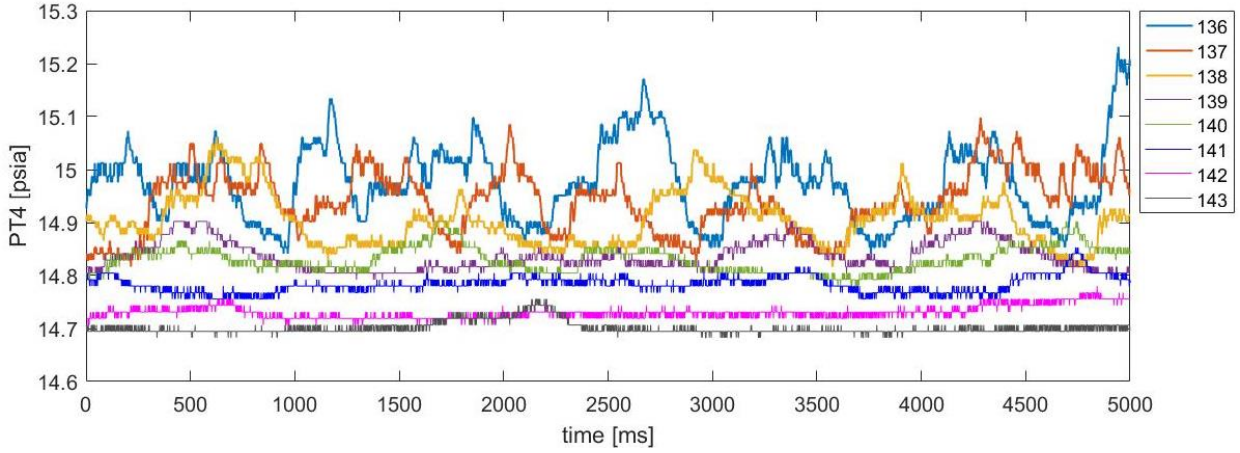

Figure 43: Section of the pressure traces for experiments 136-143.

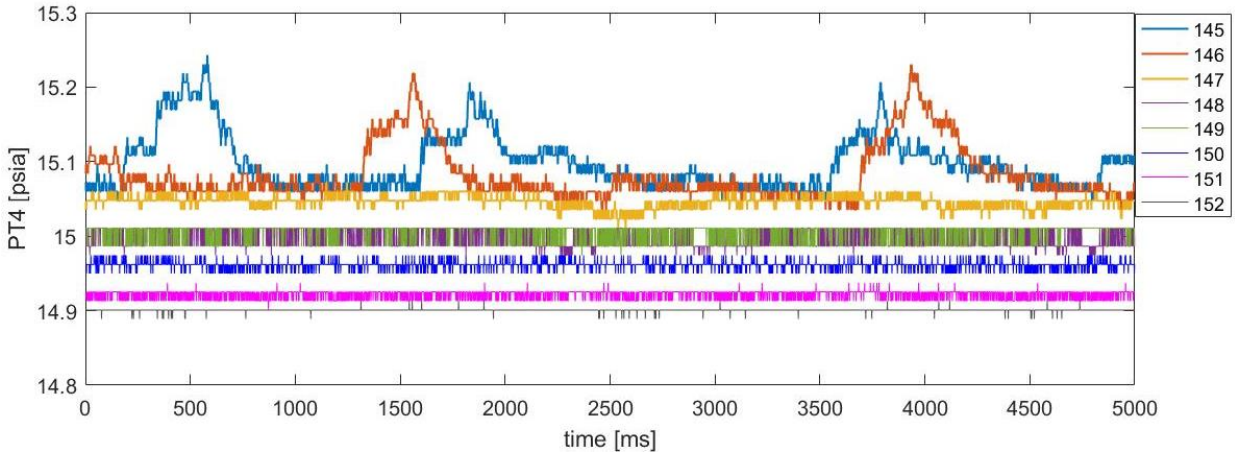

Figure 44: Section of the pressure traces for experiments 146-152.

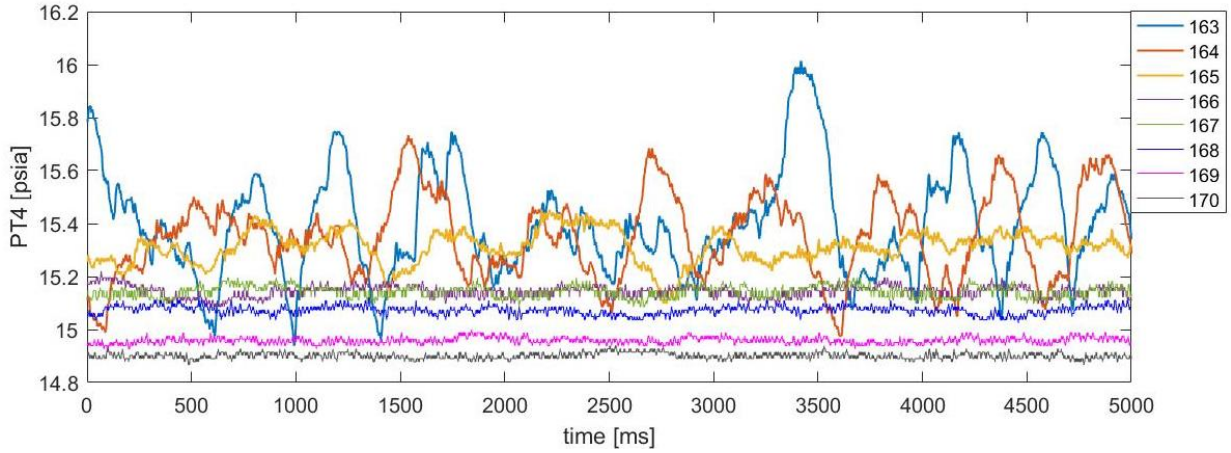

Figure 45: Section of the pressure traces for experiments 163-170.

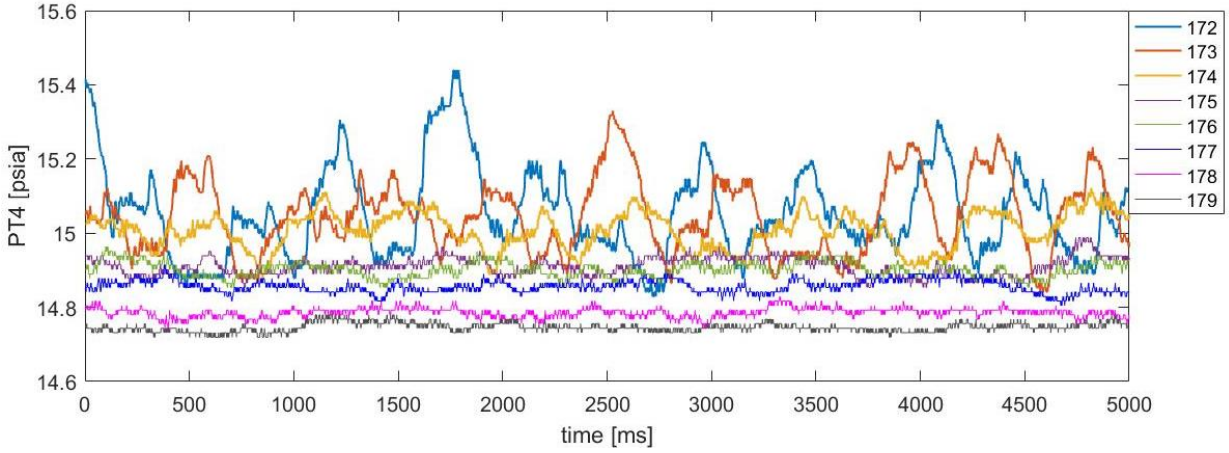

Figure 46: Section of the pressure traces for experiments 172-179.

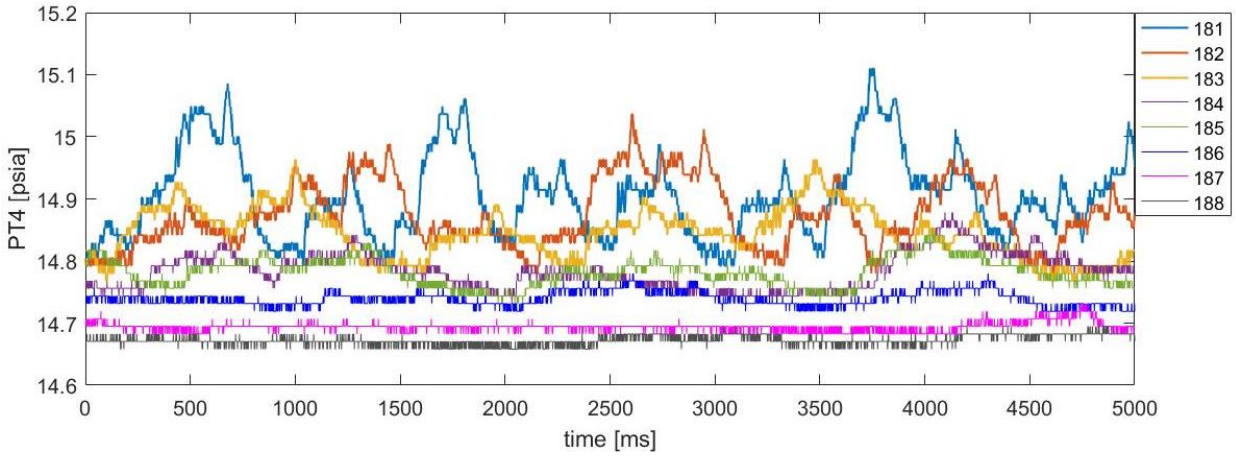

Figure 47: Section of the pressure traces for experiments 181-188.

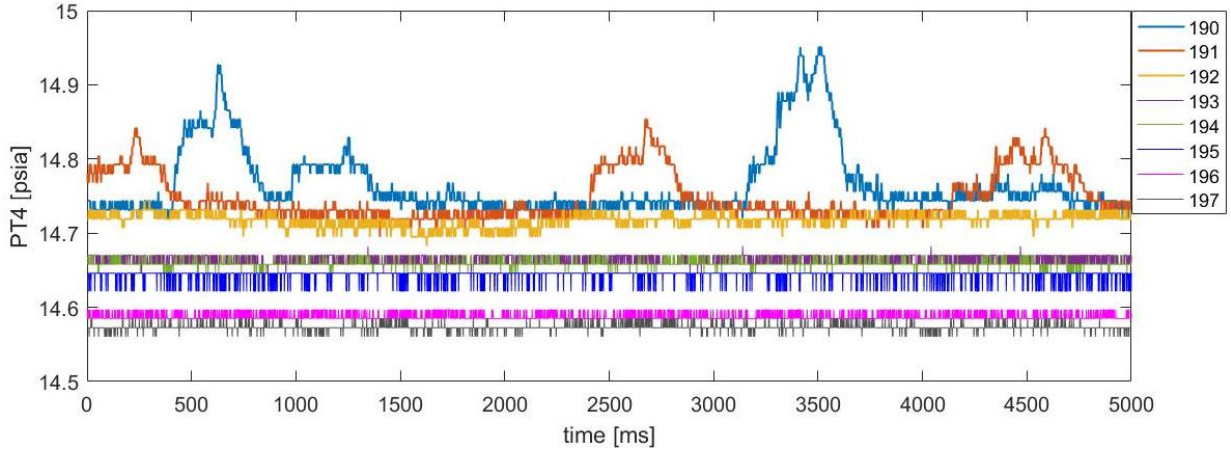

Figure 48: Section of the pressure traces for experiments 190-197.

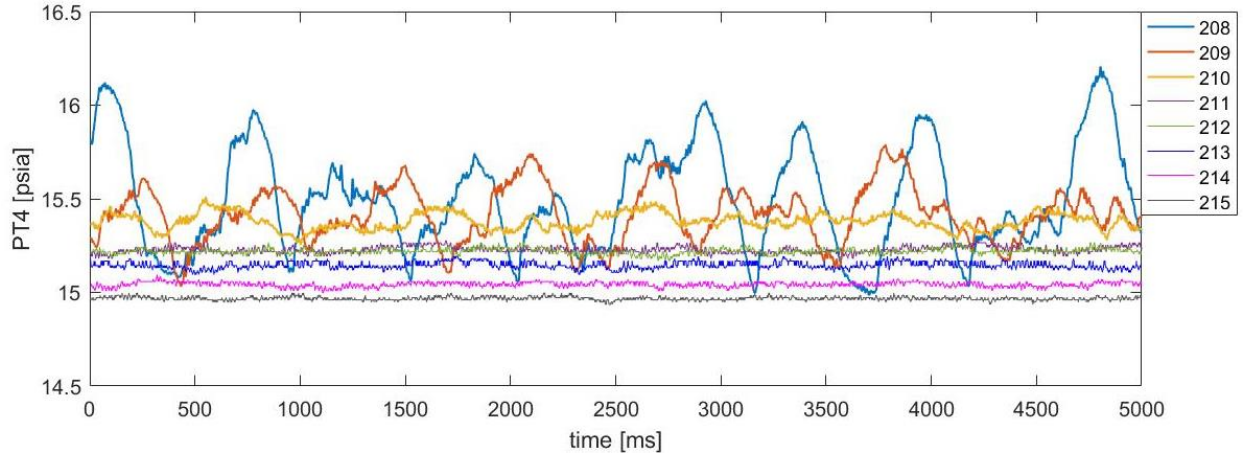

Figure 49: Section of the pressure traces for experiments 208-215.

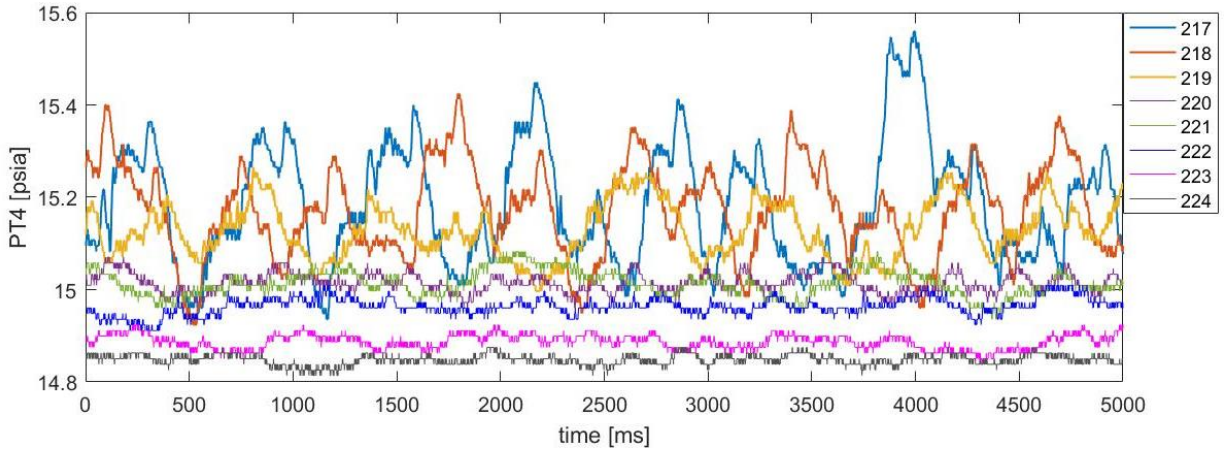

Figure 50: Section of the pressure traces for experiments 217-224.

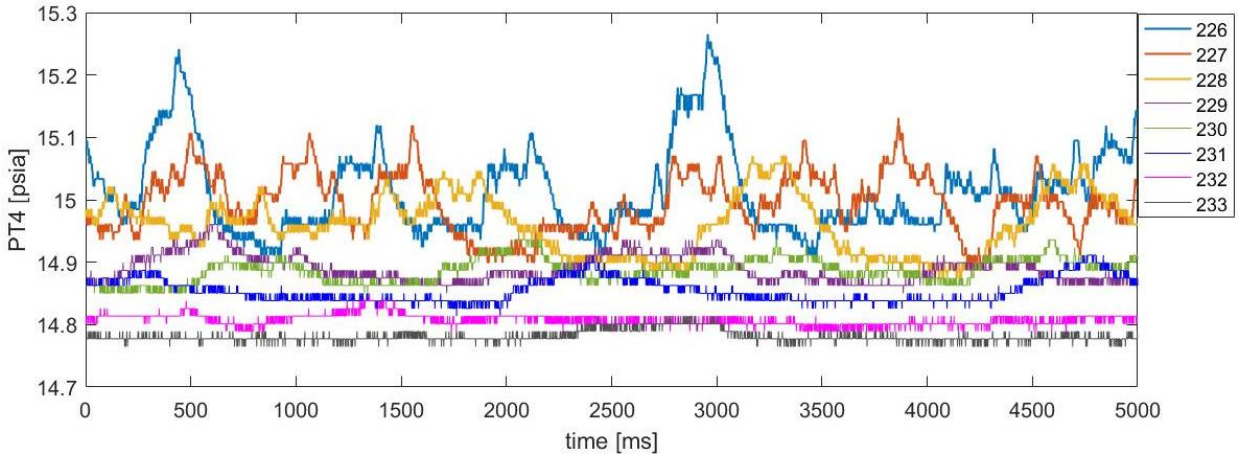

Figure 51: Section of the pressure traces for experiments 226-233.

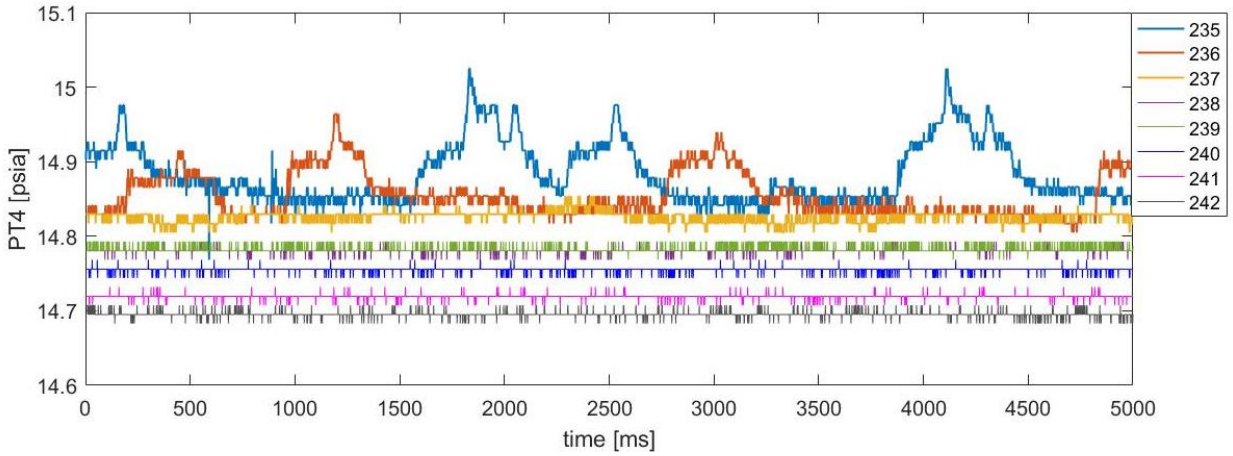

Figure 52: Section of the pressure traces for experiments 235-242.

Pressure Gradient Graphs

Figure 53, Figure 54, Figure 55, Figure 56, Figure 57, Figure 58, Figure 59, and Figure 60 are the remaining graphs from the Pressure Gradient Analysis section. The graphs followed similar trends to the graphs analyzed in the section. They were put in the Appendix so that all the data were recorded in this thesis.

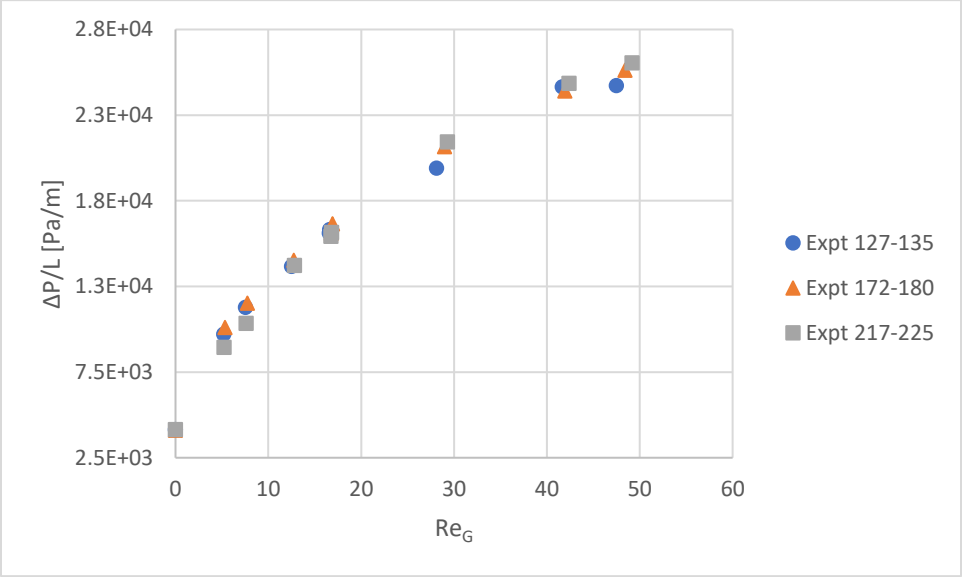

Figure 53: Pressure gradient of PT1-4 versus Re_G. The liquid rate was held constant at 2 L/min (Re_L=51.66). The flow transitioned from pulse to bubbly.

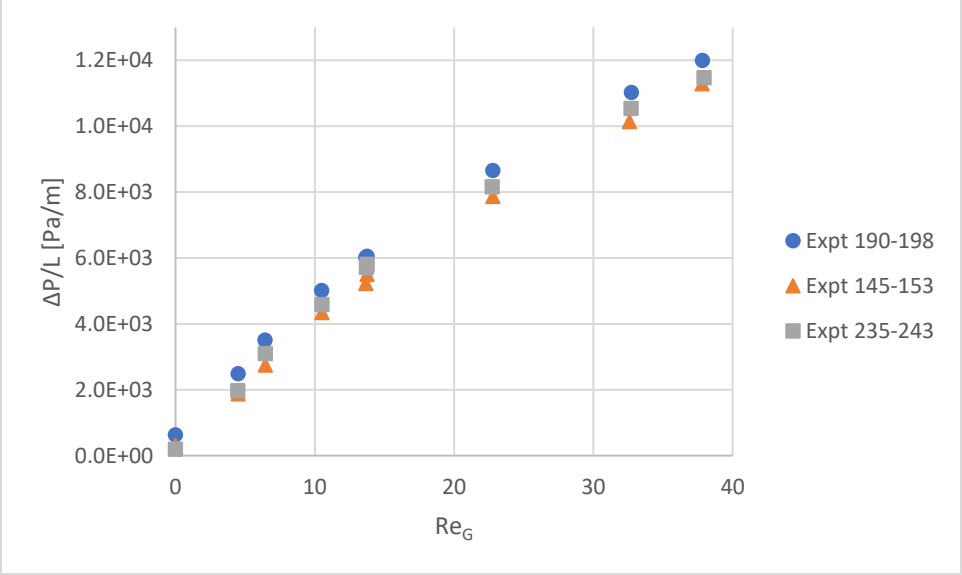

Figure 54: Pressure gradient of PT1-4 versus Re_G. The liquid rate was held constant at 1.2 L/min (Re_L=30.99). The flow transitioned from pulse to trickle.

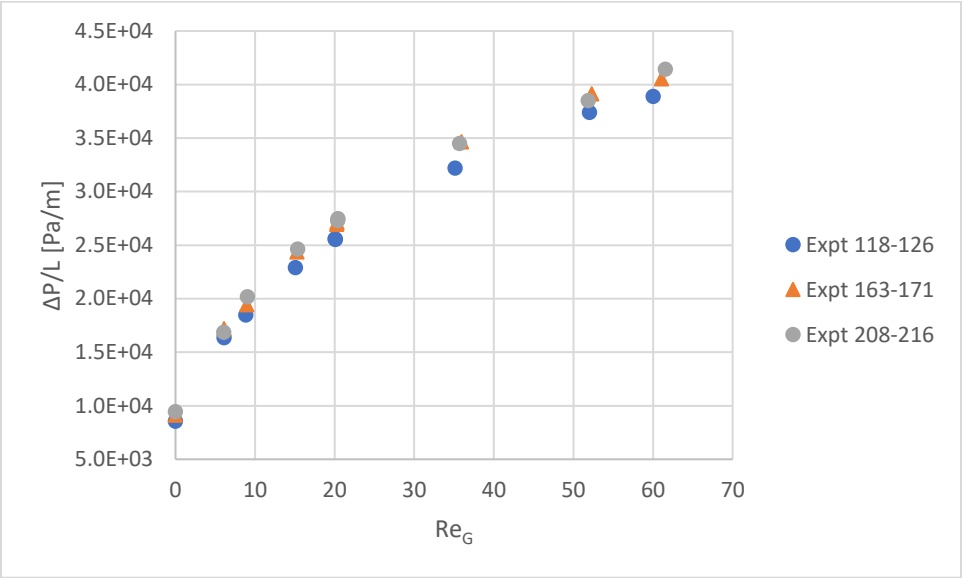

Figure 55: Pressure gradient of PT2-4 versus Re_G. The liquid rate was held constant at 3 L/min (Re_L=77.49). The flow transitioned from pulse to bubbly.

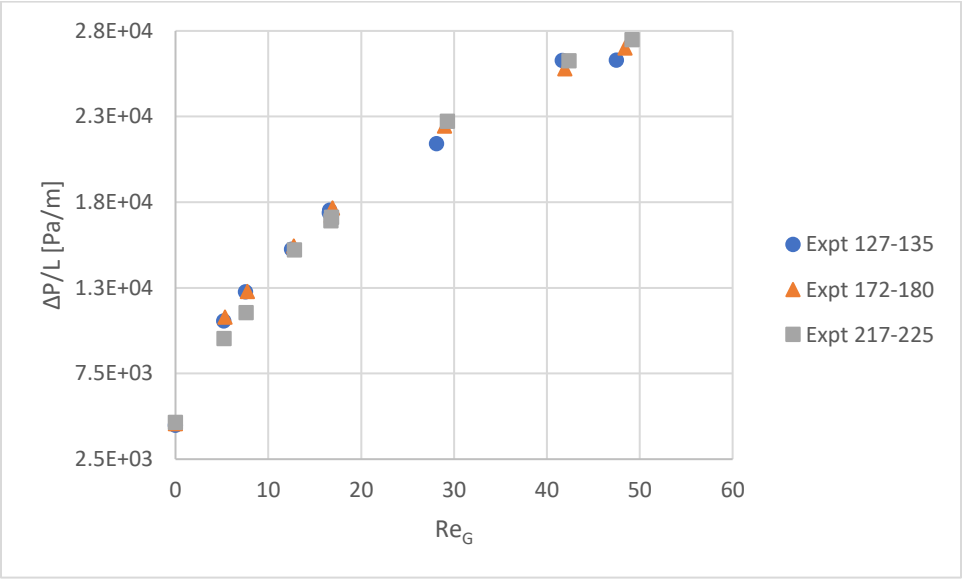

Figure 56: Pressure gradient of PT2-4 versus Re_G. The liquid rate was held constant at 2 L/min (Re_L=51.66). The flow transitioned from pulse to bubbly.

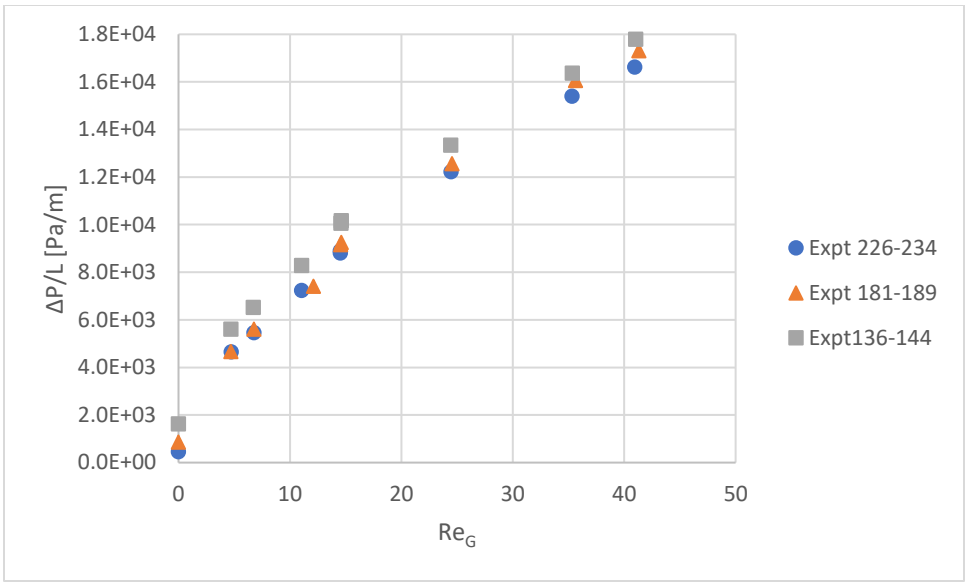

Figure 57: Pressure gradient of PT2-4 versus Re_G. The liquid rate was held constant at 1.5 L/min (Re_L=38.74). The flow transitioned from pulse to trickle.

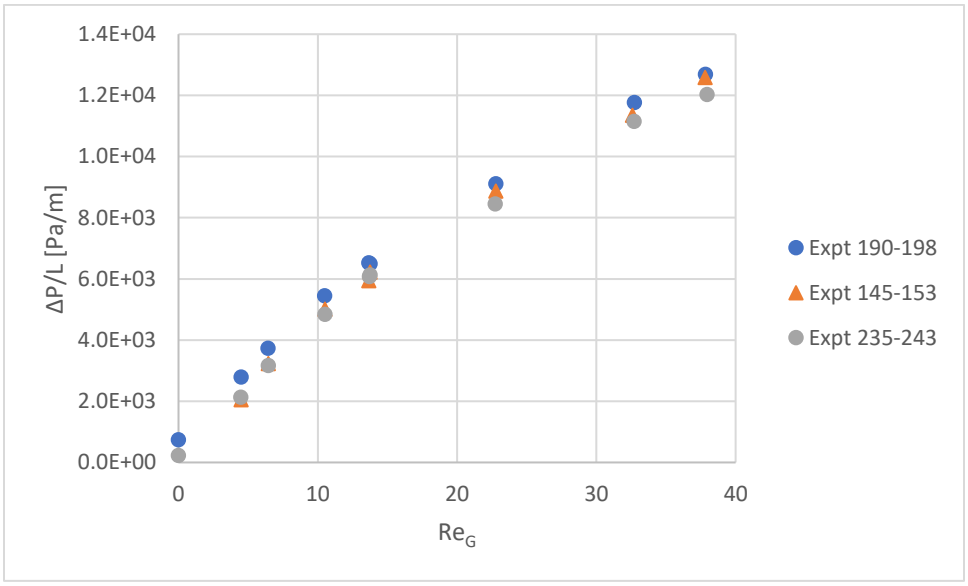

Figure 58: Pressure gradient of PT2-4 versus Re_G. The liquid rate was held constant at 1.2 L/min (Re_L=30.99). The flow transitioned from pulse to trickle.

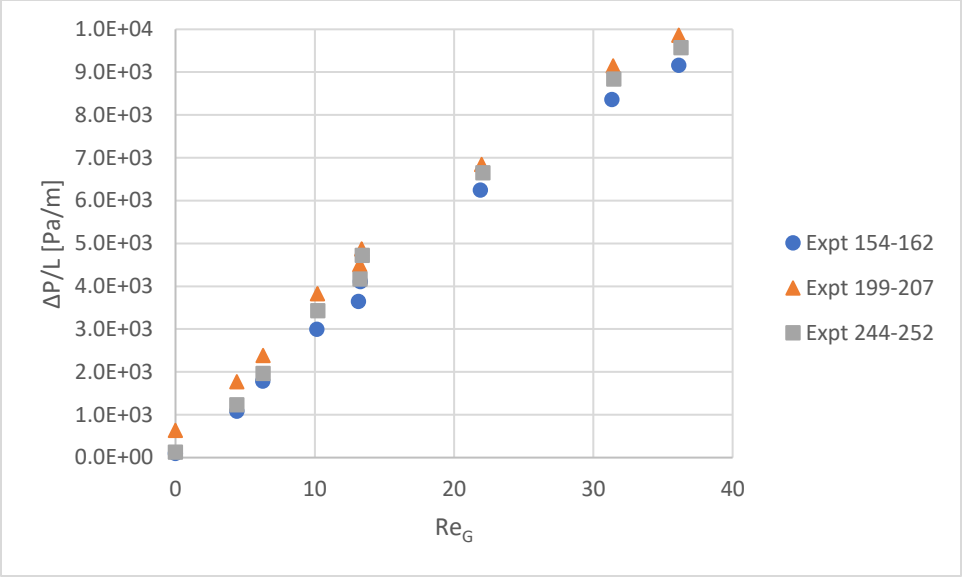

Figure 59: Pressure gradient of PT1-4 versus Re_G. The liquid rate was held constant at 1 L/min (Re_L=25.83). The flow pattern reminded trickle.

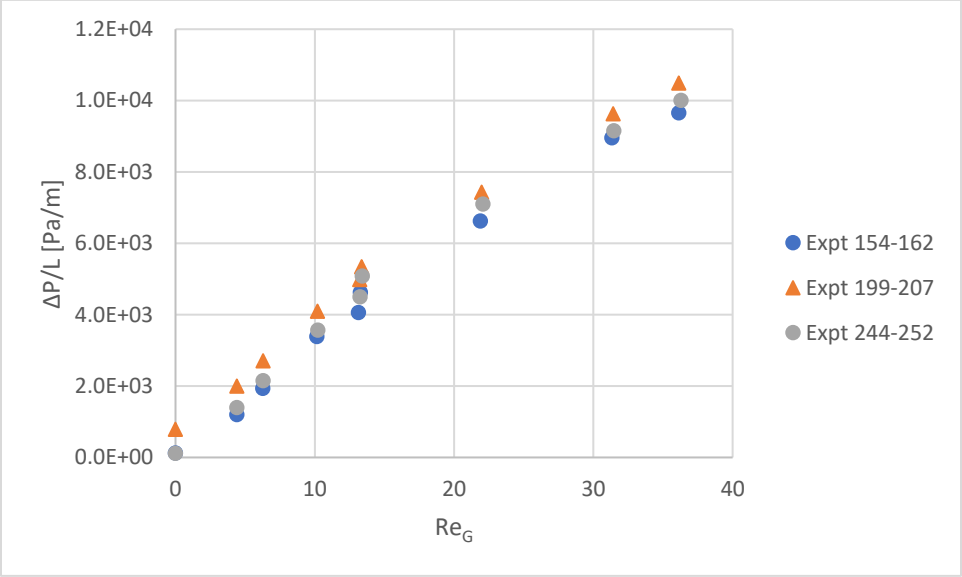

Figure 60: Pressure gradient of PT2-4 versus Re_G. The liquid rate was held constant at 1 L/min (Re_L=25.83). The flow patterned reminded trickle.

Extrapolation Curves

This section contains the remaining extrapolation curves used within the experimental calculations. Figure 61 and Figure 63 were successfully extrapolated while Figure 62 was not because any best fit curve created a negative y-intercept. The data from Figure 62 were not used in Lockhart-Martinelli calculations.

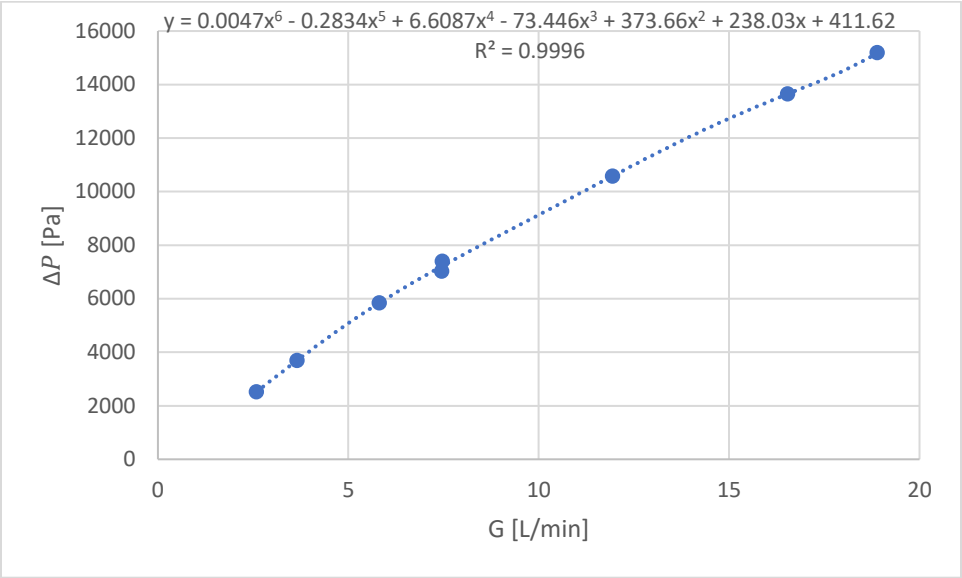

Figure 61: PT1-4 extrapolation for experiment 153. The y-intercept (411.62) was used as the liquid-only pressure instead of the negative, experimental value.

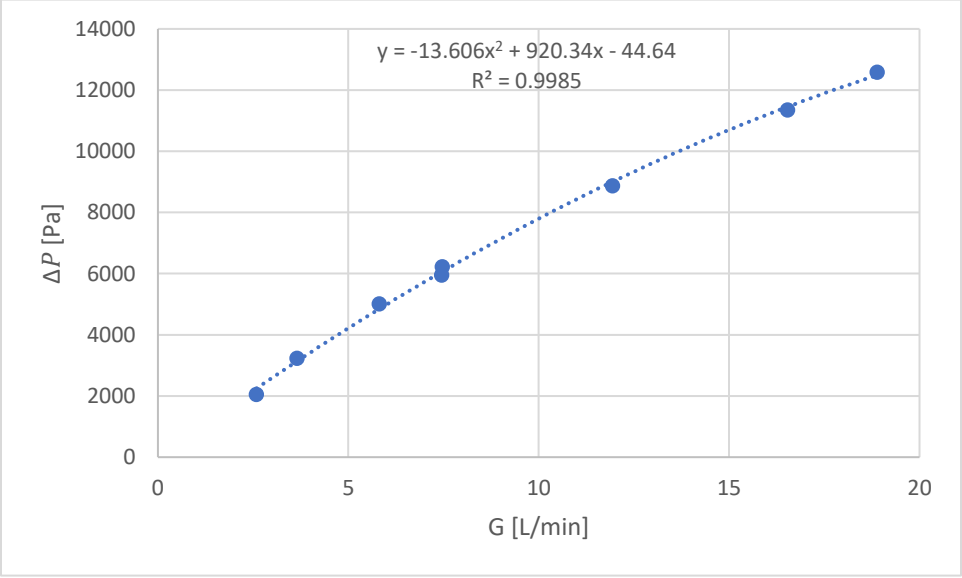

Figure 62: PT2-4 extrapolation for experiment 153. This best fit curve, along with others, produced a negative y-intercept, which defeated the purpose of extrapolating a realistic pressure. These data were not used in calculations.

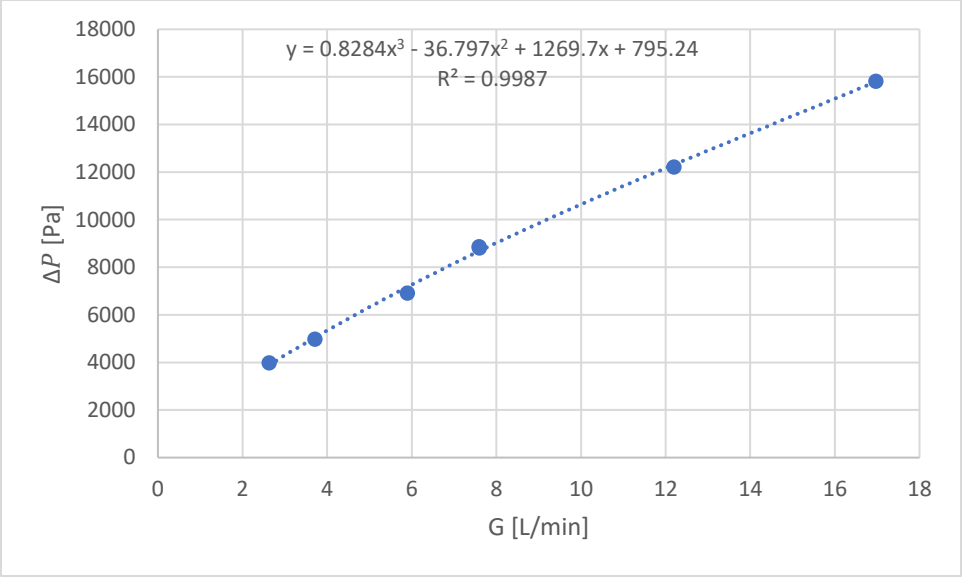

Figure 63: PT2-4 extrapolation for experiment 99. The y-intercept (795.24) was used as the liquid-only pressure instead of the negative, experimental value.

Appendix E

Cole-Palmer Calibration Curves

Figure 64, Figure 65, Figure 66, and Figure 67 are the calibration curves for each pressure transducer. The pressure transducer came pre-calibrated by Cole-Palmer.

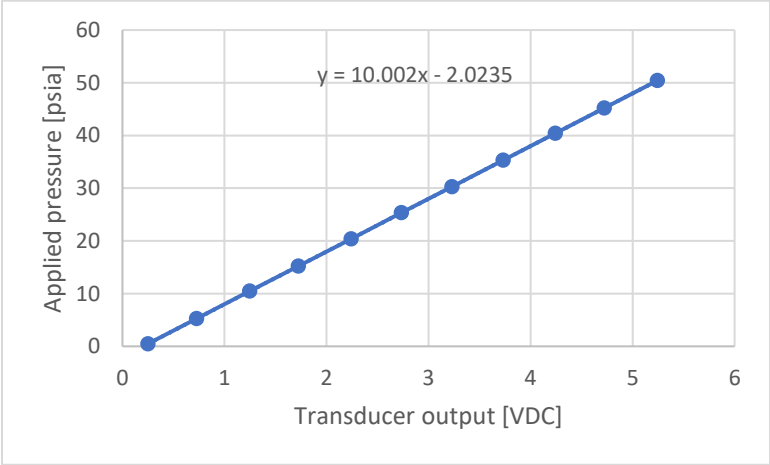

Figure 64: PT1 calibration curve provided by Cole-Palmer.

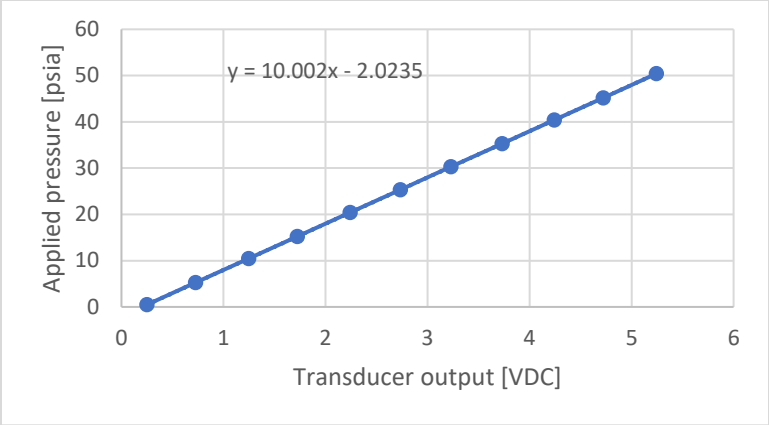

Figure 65: PT2 calibration curve provided by Cole-Palmer.

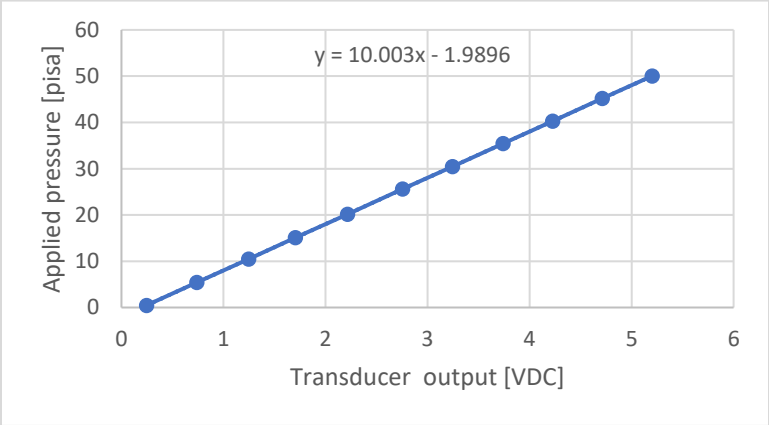

Figure 66: PT3 calibration curve provided by Cole-Palmer.

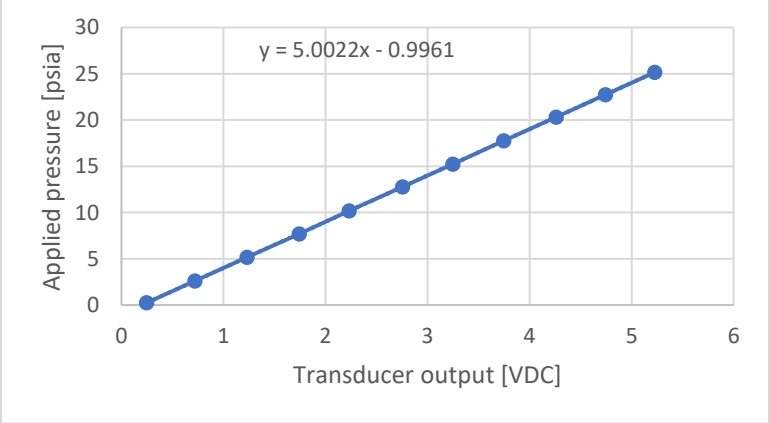

Figure 67: PT4 calibration curve provided by Cole-Palmer.